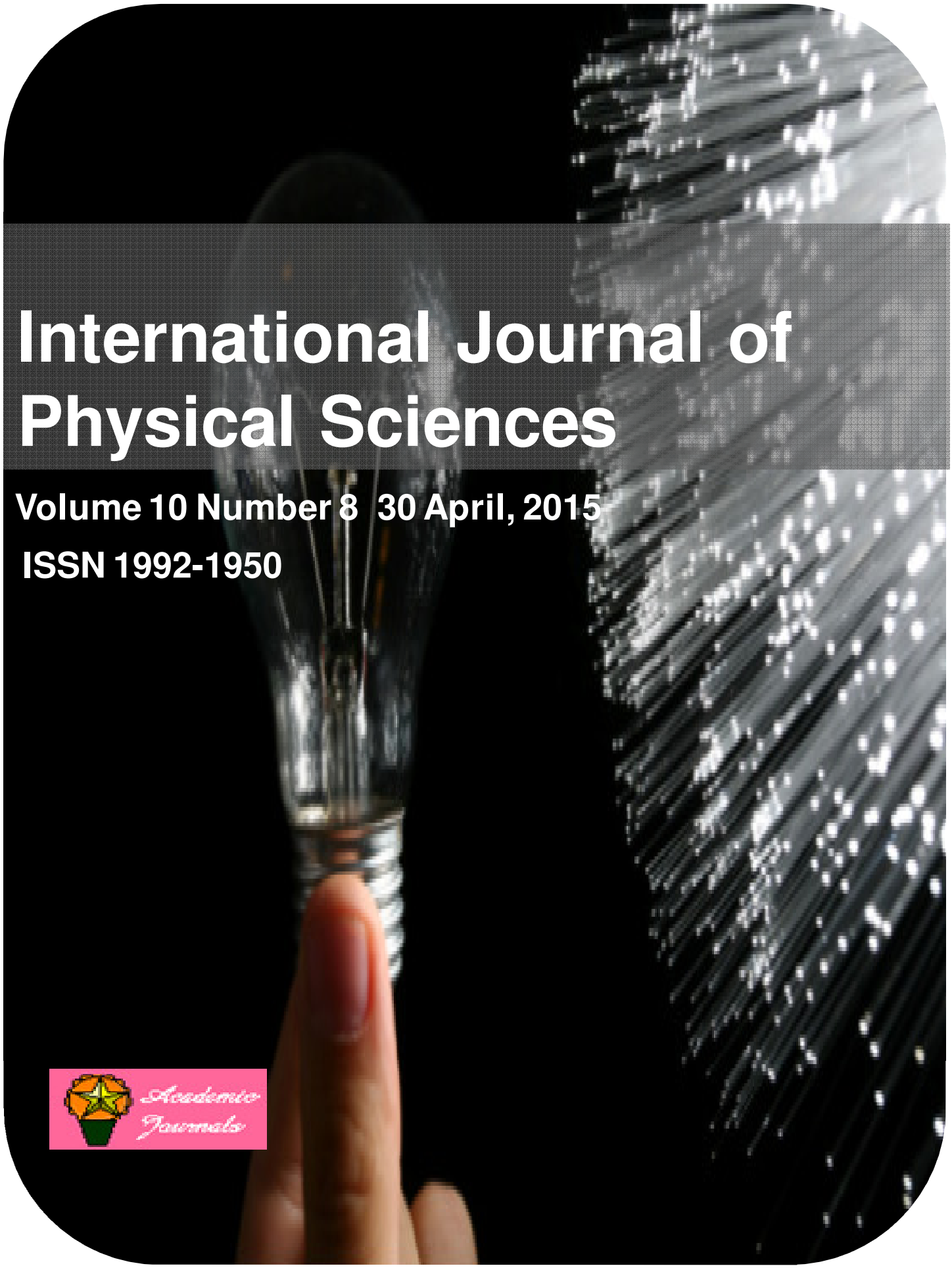

International Journal of Physical Sciences

Volume 10 Number 8 30 April, 2015

ISSN 1992-1950

Academic Journals

ABOUT IJPS

The **International Journal of Physical Sciences (IJPS)** is published weekly (one volume per year) by Academic Journals.

International Journal of Physical Sciences (IJPS) is an open access journal that publishes high-quality solicited and unsolicited articles, in English, in all Physics and chemistry including artificial intelligence, neural processing, nuclear and particle physics, geophysics, physics in medicine and biology, plasma physics, semiconductor science and technology, wireless and optical communications, materials science, energy and fuels, environmental science and technology, combinatorial chemistry, natural products, molecular therapeutics, geochemistry, cement and concrete research, metallurgy, crystallography and computer-aided materials design. All articles published in IJPS are peer-reviewed.

Contact Us

Editorial Office: ijps@academicjournals.org

Help Desk: helpdesk@academicjournals.org

Website: http://www.academicjournals.org/journal/IJPS

Submit manuscript online http://ms.academicjournals.me/

Editorial Board

International Journal of Physical Sciences

Table of Contents: Volume 10 Number 8, 30 April, 2015

ARTICLES

academicJournals

Vol. 10(8), pp. 263-269, 30 April, 2015
DOI: 10.5897/IJPS2015.4276
Article Number: FCEC51A52342
ISSN 1992 - 1950

http://www.academicjournals.org/IJPS

International Journal of Physical Sciences

Full Length Research Paper

Neutron and gamma-ray shielding properties of modified Ni- Ti- X Mo maraging steels

A. M. Reda[1,2]* and H. Halfa[3]

[1]Physics Department, Faculty of Science, Zagazig University, Zagazig, Egypt.
[2]Department of Physics, College of Science & Humanities, Shaqra University, Al-Dawadme, Saudi Arabia.
[3]Steel Technology Department, Central Metallurgical R&D Institute (CMRDI), Helwan, Egypt.

Received 5 Febraury, 2015; Accepted 25 March, 2015

MCNP5 program was used to investigate the neutron and gamma shielding properties of Ni-Ti- X Mo maraging steels. The MCNP5 program experimental setup was designed using neutrons of 14.1 MeV from sealed neutron tube and ^{60}Co as a gamma ray source. Particular attention was given to the shielding properties of neutron and gamma for low nickel free cobalt, titanium containing modified maraging steel in correlation to the molybdenum as alloying element. Based on the shielding properties, Ni-Ti- X Mo maraging steels with different molybdenum content show the same shielding properties of neutron and gamma rays when compared to the standard maraging steel 18Ni (C250). In addition, the secondary gamma ray spectra due to neutron irradiation show no obvious difference between all steels under investigation. A comparison with available calculated and experimental results of the mass attenuation coefficient at gamma energies 1173 and 1332 keV for other steels has been done. From an economic point of view newly cobalt free low-nickel maraging steel is cheaper than standard C250 maraging steel as shielding materials.

Key words: Neutron shielding, gamma ray shielding, maraging steel, MCNP5 program.

INTRODUCTION

Today, nuclear radiation has a vital role in our recent live. It has applications in many fields like medicine, industry, agriculture, archaeology, geology, academics and many others. Radiation shielding materials are required to protect the population and equipments from harmful effect of radiation. For shielding design, neutrons and gamma rays are the main types of nuclear radiation, which have to be considered, since any shield that attenuates neutrons and gamma rays will be more effective in attenuating other radiations (Yılmaz et al., 2011). Therefore, in this study, the gamma linear and mass attenuation coefficients and the effective fast neutron removal cross-section with a mass removal cross section for compounds of maraging steels (Ni-Ti- X Mo) with different molybdenum content were calculated, in addition, the secondary gamma rays emitted due to neutron interactions with these compounds have been studied. Maraging steels belong to a new class of high strength steels with the combination of strength and toughness that are among the highest attainable in general engineering alloys (Shetty et al., 2008). Voluminous experimental data have been accumulated

*Corresponding author. E-mail: amreda26@yahoo.com, Tel: +966 591511274. Fax: +966 116423708.

Table 1. The chemical composition of steels under investigation.

Steel	Chemical composition, wt%												
	C	Si	Mn	P	S	Cr	Co	Mo	Ni	Al	Ti	N	Fe
M15	0.019	0.071	0.021	0.013	0.008	0.007	-	0.007	12.0	0.06	0.0131	0.003	87.66
M19	0.015	0.185	0.099	0.02	0.010	0.007	-	4.63	12.0	0.10	0.130	0.008	82.79
M22	0.018	0.170	0.111	0.012	0.007	0.007	-	3.15	11.9	0.10	0.135	0.007	84.38
C250	0.030	0.100	0.100	0.010	0.030	-	8	3.20	18.0	0.10	0.200	0.001	70.22

on the effect of irradiation on the mechanical properties of many steels and alloys. Steels of this type with the highest strength are those containing cobalt. The use of steel with cobalt as a structural material in atomic applications is undesirable due to the high induced radioactivity under conditions of high-energy neutron bombardment. Expensive alloying additions such as Ni and Co increase the production cost for maraging steels as the cost has been the major roadblock for the widespread usage of these steels in domestic applications such as tooling, sport goods, etc. The high production cost in association with dual-use marketing issues has motivated research worldwide for cheaper alloy design. Cobalt-free maraging steels with high strength, ductility, and toughness have been developed in recent years (Hu et al., 2008; Nili-Ahmadabadi, 2008; Schnitzer et al., 2010; Leitner et al., 2011; Mahmoudi et al., 2011; Mahmudi et al., 2011; Sha et al., 2013). The best combination of properties of Maraging steel can be utilized in nuclear applications where high reliability is the principal concern. This work concerns, study the radiation resistance (neutrons and gamma rays) of low nickel titanium containing Maraging steel without cobalt and with different amounts of molybdenum in comparison with standard Maraging steel 18Ni (C250) through MCNP5 code. MCNP5 code is a general-purpose Monte Carlo radiation transport code for modeling the interaction of radiation with matter. It utilizes the nuclear cross section libraries and uses physics models for particle interactions and gives required quantity with certain error (MCNP X-5, 2003; Shultis and Faw, 2010). The neutron source used in the code is a point source which emits neutrons with energy 14.1 MeV. The two gamma energies used in the code are 1173 and 1332 keV emitted from ^{60}Co as a source of gamma rays.

EXPERIMENTAL

Material design

In this work, new developed free cobalt low nickel maraging steel with 12 mass percent nickel as base metal were designed. 12% Ni-Ti new developed maraging steel with different amounts of molybdenum were investigated. To study the radiation resistance (neutron and gamma) of new developed maraging steels, the authors also study comercial maraging steel 18Ni (C250) for the sake of comparison. Table 1 shows the chemical composition of steels under investigations.

MCNP5 experimental setup

To calculate the fast neutron removal cross section and the linear attenuation coefficient of gamma rays for maraging steels under study, two narrow beam transmission geometries were done. The first geometry, for neutron, Figure 1(a) shows a lead box of 3 x 3 x 3 m^3 dimensions as a neutron source housing with a cylinder collimator of 1 cm radius. The detector was put on the same line at a distance 61 cm from neutron source. The detector collimator has an aperture of 1 cm radius and 5 cm thickness. The investigated materials were put between the source and the detector at a distance 40 cm from the source. The materials under investigation were a cylinder of 3 cm radius and thicknesses with 2, 5, 10 and 15 cm. Tally type 4 was used to count the number of neutrons inter the detector per MeV. cm^2. s^{-1}. The number of histories used in the code in the neutron case is 30 x 10^6. The estimated statistical error in all neutron energy bens with these numbers of histories not exceed 10%. Also, The error in the energy bens of secondary gamma rays not exceed 0.05%. The second geometry, for gamma, Figure 1(b) shows the ^{60}Co house box with dimensions 15 x 30 x 30 cm^3 made of lead and coated by 0.5 cm thickness of steel. A cone lead collimator was put between the source and the investigated material with 15 cm length, end opening of 0.5 cm radius and also coated with 0.5 cm of steel. The investigated materials were put between the source and the detector at a distance 22.5 cm from the source and have the same dimensions as in neutron geometry. The gamma detector was put on the same line in front of a gamma source at a distance 44.5 cm from it. The detector shield face was 39.5 cm from the source with opening radius 0.5 cm. The same tally type 4 was used to estimate gamma photons registered in the detector per MeV. cm^2. s^{-1}. The number of histories used in the code is 20 x 10^6. The statistical error in the calculated data not exceed 0.05% for each gamma energy.

RESULTS AND DISCUSSION

Neutron shielding properties

Neutron attenuation through the investigated materials have been calculated by performing the transmission experiment in narrow beam geometry shown in Figure 1(a). Figure 2 shows the neutron flux transmitted to the detector in case of no material and the neutron flux transmitted through 2, 5, 10 and 15 cm thicknesses of the different shielding materials under investigation. The figure shows that, the fast neutrons were moderated and moves from its higher group to a group of less energy. The number of moderated neutrons was increased with

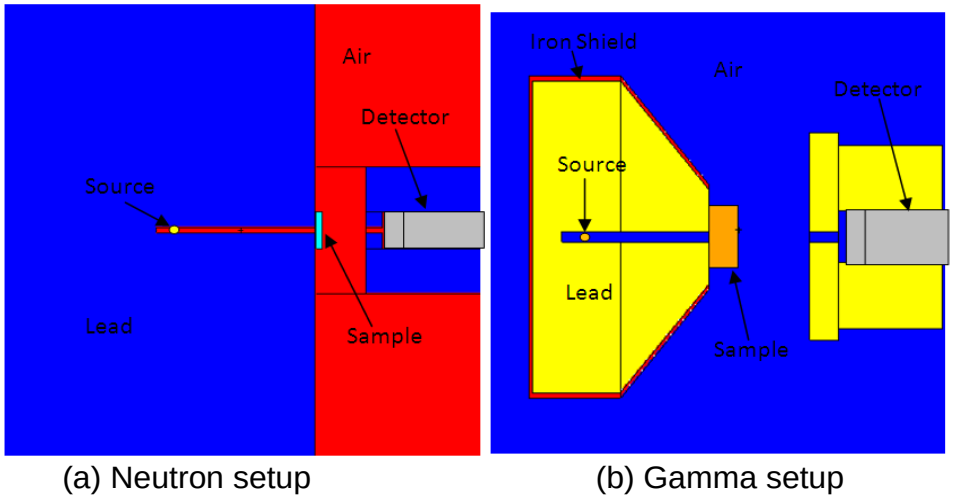

Figure 1. Experimental setup for measuring effective fast neutron removal cross-section (a) and gamma linear attenuation coefficient (b).

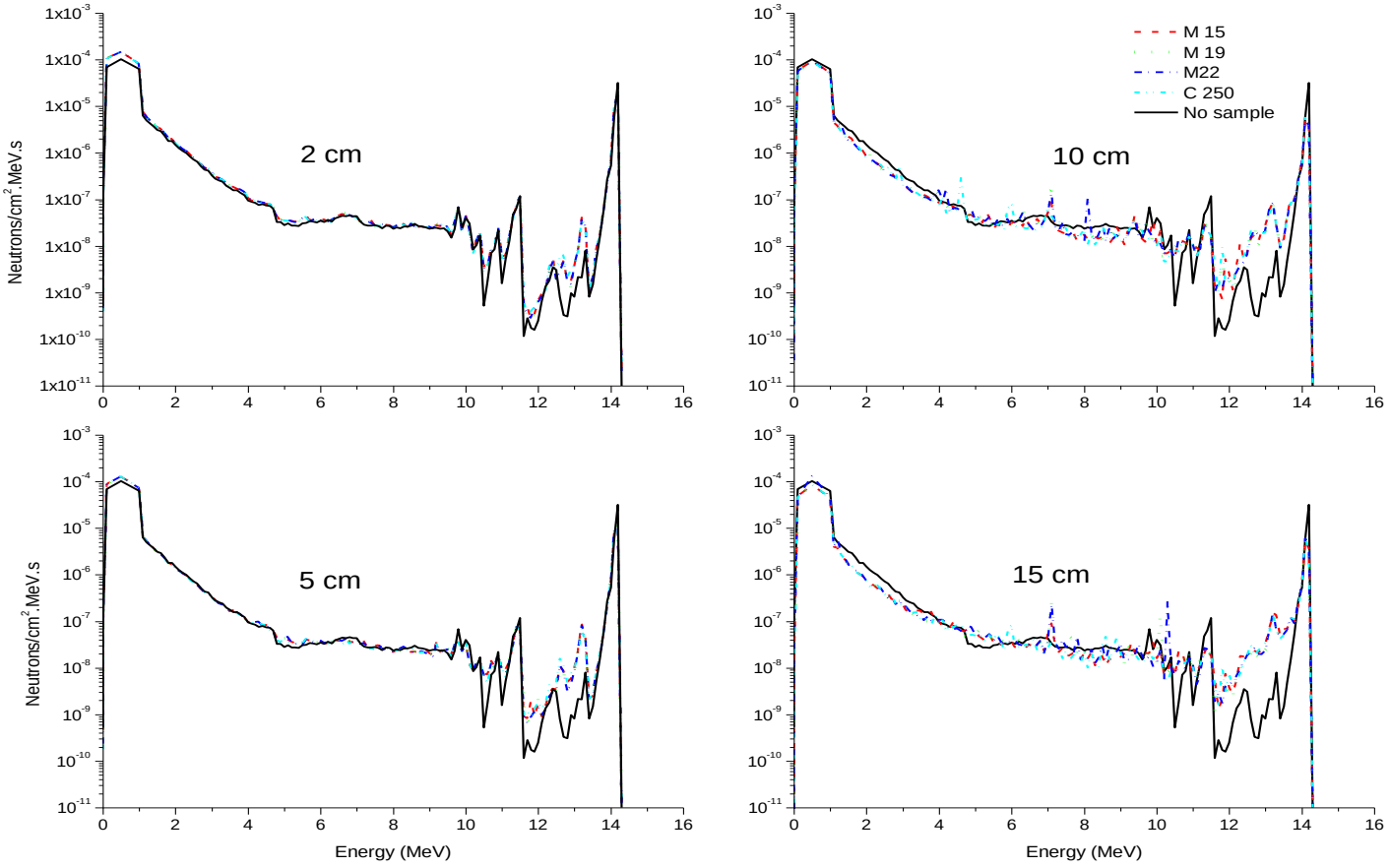

Figure 2. Transmitted neutron spectra versus neutron energy at different thickness of the investigated steels in comparison with neutron spectra without sample (black line).

shielding material thickness increased. The important is that, the neutron moderation ratio for the different steels and for the compared steel C250 is the same. This result was insured by calculating the effective fast neutron

Table 2. Effective fast removal cross section Σ_R (cm^{-1}) and mass removal cross section Σ_R/ρ (cm^2/g) for steels under study.

	Steel No.			
	M15	**M19**	**M22**	**C250**
Σ_R (cm^{-1})	0.4976E-01	0.5038E-01	0.5073E-01	0.5287E-01
Σ_R/ρ (cm^2/g)	0.6332E-02	0.6411E-02	0.6455E-02	0.6727E-02

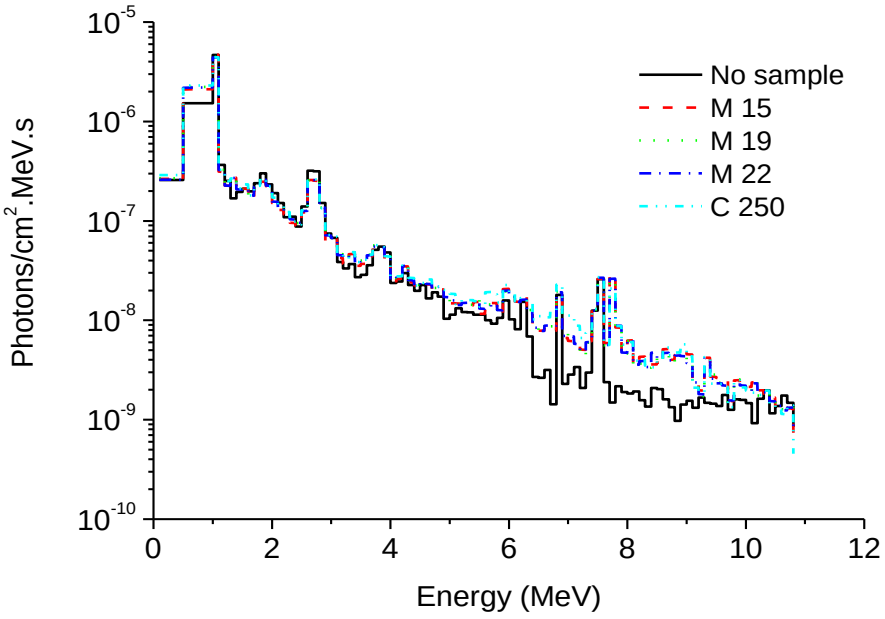

Figure 3. Secondary gamma ray spectra arising from neutron interactions with under investigation steels.

removal cross section $\sum_R$ (cm^{-1}) which obtained by the equation $\sum_R = \frac{ln\frac{I_0}{I}}{x}$ where I and I_0 are the neutron intensity with and without the material between the neutron source and the detector respectively and x is the material thickness. Therefore, plotting each $ln\frac{I_0}{I}$ versus x, the slope of the straight line obtained is the value $\sum_R$ of the material. The obtained effective fast neutron removal cross section $\sum_R$ (cm^{-1}) and the mass removal cross section $\boldsymbol{\Sigma}_R/\rho$ (cm^2/g) for the investigated materials are tabulated in Table 2 with the values of standard steel for comparison. As shown in the table, the produced steels have approximately the same values of effective and mass removal cross-section and as the values of the standard material C250. This means that, our produced steels work as neutron shielding material and have the same neutron attenuation in comparison with the standard.

Secondary gamma rays

Interaction of neutrons with elements constitute the material produce secondary gamma-rays. Figure 3 shows the spectra of gamma-rays produced due to interactions of neutrons with 2 cm thickness of steels under investigation including the standard. There are no appear signals for gamma coming from the cobalt present in the standard sample C250 as expected. This can be explained by, the number of neutrons which moderated and arrived to thermal neutrons is a very modest number due to the small thicknesses used in the study. In addition, the self shielding of the material makes it absorb some of produced gamma rays specially low energy gamma like that produced from neutron interaction with cobalt (1173 and 1332 keV). Also, the figure shows an increase in secondary gamma for the standard steel in the energy range from 5.5 to 8 MeV more than others. Figure 4 shows the integral flux of secondary gamma versus the material thickness of all investigated materials. As shown in figure the integral flux decreases exponentially with material thickness increase.

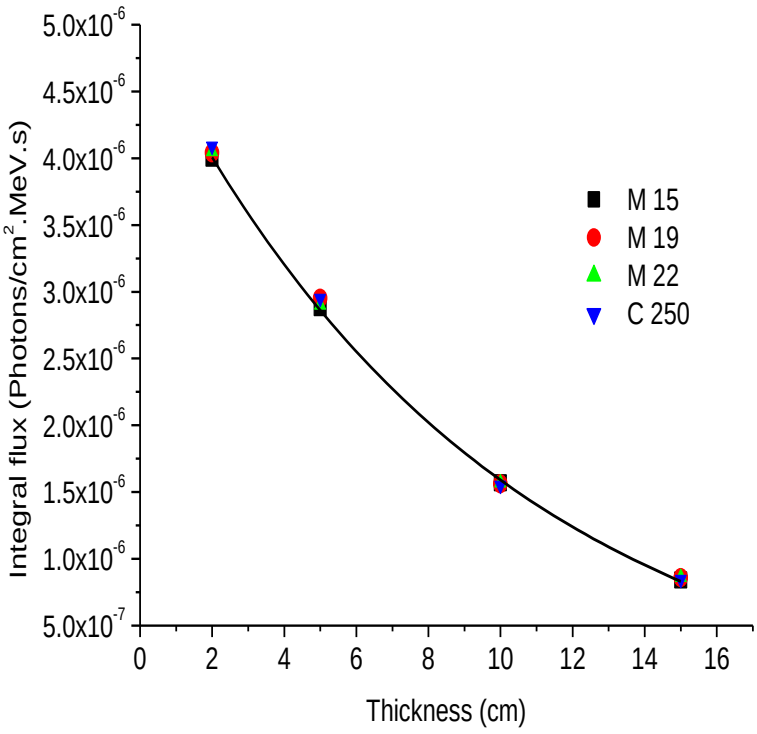

Figure 4. Integral flux of secondary gamma versus shielding material thickness of all studied materials.

This is because, the most number of neutrons interact through the first layers of shielding materials and produce secondary gamma rays which shielded from the residual layers of the material itself. An empirical equation for the emitted secondary gamma rays versus material thickness can be deduce in the form $\emptyset = ae^{-bx}$ where, $\emptyset$ is the integral flux of secondary photons and x is the material thickness and a, b are constants for the material type.

Gamma ray shielding properties

Narrow beam geometry shown in Figure 1(b) was used to study gamma ray attenuation through our materials and through the standard one. Figure 5 shows ^{60}Co gamma ray spectra transmitted through 2, 5, 10 and 15 cm thickness of the investigated materials with gamma spectra transmitted directly without material between the source and the detector. As shown in the figure, for all materials there is no obvious difference in the values of gamma attenuation. Also, when material thickness increase gamma intensity decrease. Intensity of the two gamma lines 1173 and 1332 KeV which collected under energy bins 1200 and 1350 KeV respectively were calculated versus the material thicknesses. As in the case of neutron, the gamma linear attenuation coefficient μ (cm^{-1}) of the two gamma lines for materials can be calculated from the equation $\mu = \frac{ln\frac{I_0}{I}}{x}$ where I, I_0 are the gamma line intensity with and without the material and x is the material thickness. Hence, plotting each $ln\frac{I_0}{I}$ versus x for each gamma line, the slopes of the two straight lines obtained are the values μ of the material for these two energy lines. The values of gamma linear attenuation coefficient μ (cm^{-1}) and mass attenuation coefficient μ (cm^2/g) of the materials for the two gamma lines are summarized in Table 3. The tabulated data show the obvious approximation between the investigated materials in attenuation of gamma rays. Also, there is no difference between standard steel and the investigated materials in gamma attenuation.

The results of the present simulation of the mass attenuation coefficient at energies 1173 and 1332 keV were compared with the experimental results of different steels (Akkurt, 2009; EL-Kameesy et al., 2011). In addition, the present results were compared with the theoretical and simulated results of WinXcom, Geant4 and MCNP (Singh et al., 2015) for steel 1. The chemical composition of compared steels is shown in Table 4. Table 5 shows the results of the present work and the possible experimental and calculated data reported in the mentioned different literatures. As shown in Table 5 the results of the present study agree with the theoretical

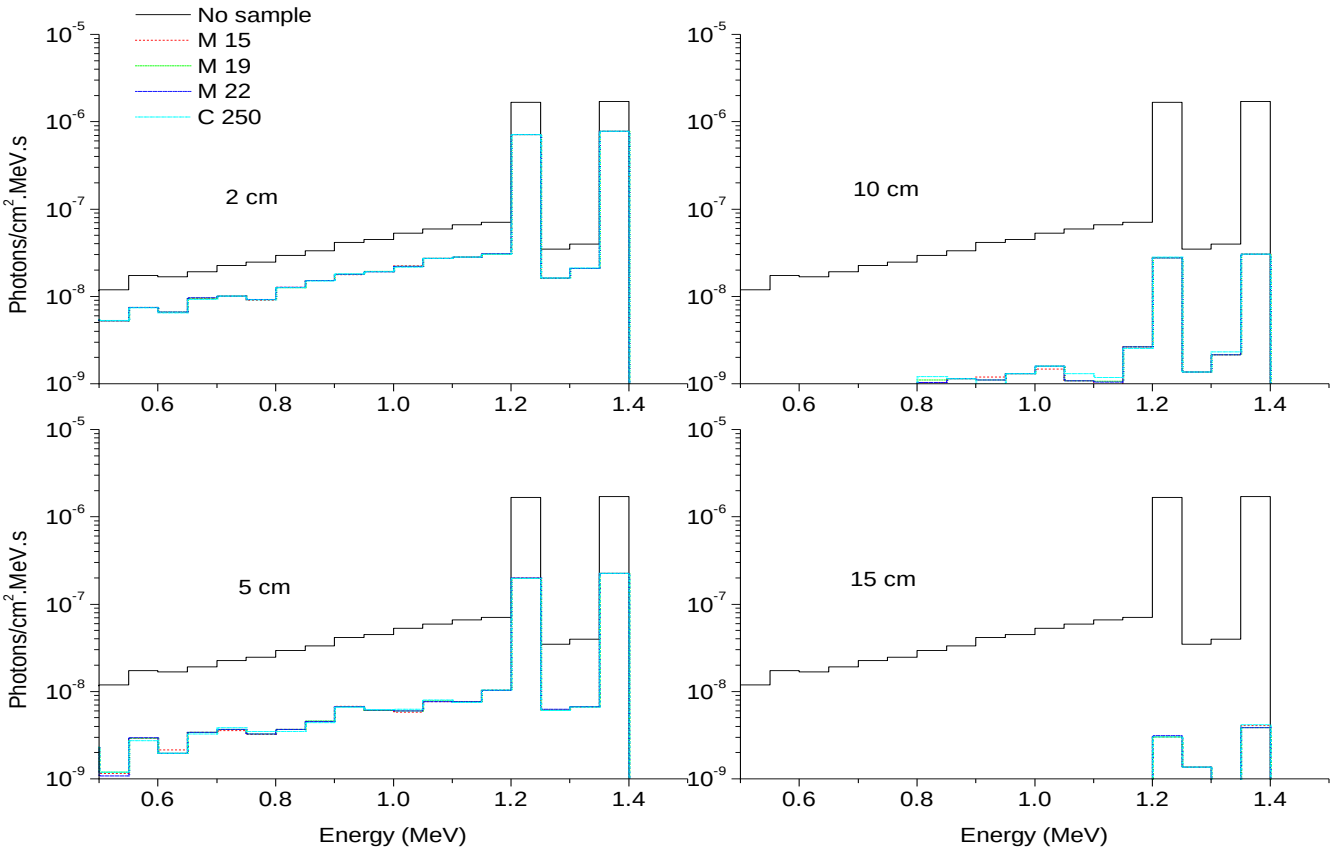

Figure 5. Gamma ray spectra transmitted to the detector in present of shielding materials with different thicknesses compared with no shielding materials.

Table 3. Gamma linear attenuation coefficient μ (cm^{-1}) and mass attenuation coefficient μ/ρ (cm^2/g) for steels under investigation.

Steel No.	Eγ=1173 KeV		Eγ=1332 KeV	
	μ (cm^{-1})	μ/ρ (cm^2/g)	μ (cm^{-1})	μ/ρ (cm^2/g)
M15	4.1903E-01	5.3311E-02	4.0301E-01	5.1274E-02
M19	4.1992E-01	5.3424E-02	4.0460E-01	5.1475E-02
M22	4.1913E-01	5.3324E-02	4.0446E-01	5.1458E-02
C250	4.1958E-01	5.3382E-02	4.0301E-01	5.1273E-02

WinXcom and simulated Geant4, MCNP results for steel 1. The difference from the experimental results may be due to the setup of the experiments and the steel density, in addition to the difference in compounds of the steels.

Conclusion

The produced steels have the same ability to moderate neutrons and to attenuate gamma rays in comparison with C250 Maraging steel. The problem of secondary gamma rays produced due to neutron interactions with steel can be solved with higher material thickness, where there is an exponential relation between secondary gamma and the material thickness due to the material self shielding. The results of gamma ray mass attenuation coefficient at energies 1173 keV and 1332 KeV for steels under investigation were found comparable with experimental results, the theoretical WinXcom, the Geant4 and MCNP simulation values of others steels. From economical point of view, newly modified Maraging steel with previous shielding properties are promising material in shielding applications. Future work should be done to study neutron shielding properties and neutron reflection characteristics at higher thicknesses and at higher temperature for the produced steels to be used as a nuclear reactor vessel.

Table 4. The chemical composition of comparative steels (Akkurt, 2009; EL-Kameesy et al., 2011; Singh et al., 2015).

	Chemical composition. wt%														
Steel	**C**	**Si**	**Mn**	**P**	**S**	**Cr**	**Co**	**Mo**	**Ni**	**Al**	**Ti**	**N**	**Cu**	**W**	**Fe**
S1	0.1200	0.37	1.00	0.024	0.005	17.0	0.07	0.630	6.86	-	-	-	0.210	-	73.70
S2	0.9000	-	-	-	-	4.10	-	5.000	-	-	-	-	-	6.4	83.70
S3	0.1200	0.05	0.28	0.060	0.008	0.02	-	0.005	0.013	-	-	-	-	-	98.50
Steel 19	0.0102	-	-	-	-	3.71	-	3.190	12.03	-	0.0250	-	-	-	81.03
Steel 21	0.0880	-	-	-	-	4.36	-	3.180	12.16	-	0.0400	-	-	-	80.17
Steel 12	0.0169	-	-	-	-	5.04	-	2.870	12.12	-	0.0300	-	-	-	79.92
Steel 1	0.4200	0.25	0.89	0.021	0.110	1.05	-	0.200	0.06	0.049	0.0019	-	0.010	-	97.03

Table 5. The mass attenuation coefficient at energies 1173 keV and 1332 keV for the steels under investigation and the comparative steels (Akkurt, 2009; EL-Kameesy et al., 2011; Singh et al., 2015) for the sake of comparison.

Energy (keV)	**Present study**				**Experimental (Akkurt, 2009)**			**Experimental (EL-Kameesy et al., 2011)**			**Theoretical and simulated (Singh et al., 2015)**
	M15	**M19**	**M22**	**C250**	**S1**	**S2**	**S3**	**Steel 19**	**Steel 21**	**Steel 12**	**Steel 1**
1173	5.331E-02	5.342E-02	5.332E-02	5.338E-02	4.84E-02	4.449E-02	7.141E-02	6.700E-02	7.247E-02	7.081E-02	5.490E-02
1332	5.127E-02	5.147E-02	5.145E-02	5.127E-02	3.25E-02	3.336E-02	6.664E-02	6.245E-02	6.521E-02	6.360E-02	5.120E-02

Conflict of Interest

The authors have not declared any conflict of interest.

REFERENCES

Akkurt I (2009). “Effective atomic and electron numbers of some steels at different energies”. Ann. Nuclear Energy. 36:1702–1705.

EL-Kameesy SU, Halfa H, EL-Gammam YA (2011). “Maraging steel as a gamma rays shielding material”. Isotope Radiat. Res. 43(3):717-725.

Hu ZF, Mo DF, Wang CX, He GQ, Chen SC (2008). “Different behavior in electron beam welding of 18Ni Co-free maraging steels”. J. Mater. Eng. Perform. 17(5):767-771.

Leitner H, Schober M, Schnitzer R, Zinner S (2011). “Strengthening behavior of Fe-Cr-Ni-Al-(Ti) maraging steels”. Mater. Sci. Eng. A. 528(15):5264-5270.

Mahmoudi A, Ghavidel MRZ, Nedjad SH, Heidarzadeh A, Ahmadabadi MN (2011). “Aging behavior and mechanical properties of maraging steels in the presence of submicrocrystalline Laves phase particles”. Mater. Characterization. 62(10):976-981.

Mahmudi A, Nedjad SH, Behnam MMJ (2011). “Effects of cold rolling on the microstructure and mechanical properties of Fe- Ni-Mn-Mo-Ti-Cr maraging steels”. Int. J. Minerals, Metallurgy Mater. 18(5):557-561.

MCNP X-5 (2003). "A General Monte Carlo N-Particle Transport Code: V. 5,vol. I (LA-UR-03e1987) and vol. II (LA-CP-0245)". Los Alamos National Laboratory.

Nili-Ahmadabadi M (2008). “Improvement in mechanical properties of Fe-Ni-Mn maraging steel by heavy cold rolling”. Int. J. Modern Phys. B. 22(18-19):2814-2822.

Schnitzer R, Schober M, Zinner S, Leitner H (2010). “Effect of Cu on the evolution of precipitation in an Fe-Cr-Ni-Al-Ti maraging steel”. Acta Mater. 58(10):3733-3741.

Sha W, Chen Z, Geriletu XXX, Lee JS, Malinov S, Wilson EA (2013). “Tensile and impact properties of low nickel maraging steel”. Mater. Sci. Eng. A. 587:301-303.

Shetty K, Kumar S, Rao PR (2008). “ Ion-nitriding of Maraging steel (250 Grade) for Aeronautical application”. J. Phys. Conf. Series. 100-062013.

Shultis JK, Faw RE (2010). "An MCNP PRIMER Department of Mechanical and Nuclear Engineering". Kansas State University.

Singh VP, Medhat ME, Shirmardi SP (2015). “Comparative studies on shielding properties of some steel alloys using Geant4, MCNP, WinXCOM and experimental results”. Radiation Phys. Chem. 106:255–260.

Yılmaz E, Baltas H, Kırıs E, Ustabas I, Cevik U, El-Khayatt AM (2011). "Gamma ray and neutron shielding properties of some concrete materials". Ann. Nuclear Energy. 38:2204-2212.

academicJournals

Vol. 10(8), pp. 270-275, 30 April, 2015
DOI: 10.5897/IJPS2015.4260
Article Number: B832CE052346
ISSN 1992 - 1950

http://www.academicjournals.org/IJPS

International Journal of Physical Sciences

Full Length Research Paper

Two methods for extracting the parameters of a non-ideal diode

M. Khalis[1], R. Masrour[2,3]*, Y. Mir[1] and M. Zazoui[1]

[1]Laboratory of Condensed Matter, Faculty of Sciences and Techniques, University of Hassan II Mohammedia, Casablanca, Avenue Hassan II, BP 146, 28800 Mohammedia, Morocco.
[2]Laboratory of Materials, Processes, Environment and Quality, Cady Ayyed University, National School of Applied Sciences, Safi, Morocco.
[3]LMPHE (URAC 12), Department of Physics, B.P. 1014, Faculty of Science, Mohammed V-Agdal University, Rabat, Morocco.

Received 15 January, 2015; Accepted 26 March, 2015

We describe two methods of extracting physical parameters of a non ideal p-n diodes. These include the ideality factor, saturation current and series resistance. The proposed techniques that treat extraction parameters, using the current-voltage characteristic (I,V) forward biased. The first method is to learn three different points of the curve, with the coordinates of these points, one can generate a system of nonlinear equations expressing the electrical parameters. The resolution of these non-linear equations was performed by the numerical method of Newton-Raphson. The second is based on the least squares method. Both methods are tested using programs developed in Matlab code based on the experimental characteristic (I-V) of two different diodes in silicon.

Key words: Diode characteristic, electrical parameters, w-function Lambert, equations of non-linear system, method of least squares.

INTRODUCTION

Photovoltaic (PV) cells are the elementary components of a PV generator and their electrical properties are exhibited nonlinear in light of recent research results (Masoum et al., 2002). A commercial PV module is composed of a series of PV cells connected electrically. In view of the fact that the power generated by PV modules is heavily dependent on a number of atmospheric conditions (e.g. temperature and solar irradiance), the efficiency of energy conversion has drawn the most attention in PV system design (Hussein et al., 1995; Chun and Kwasinski, 2011; Kumar and Panchal, 2013). The solar cell behavior under illumination is interpreted by several models; whose the equivalent electrical circuit based on single diode is the most widely used (Kumar and Panchal, 2013; Fathabadi, 2013; Rajasekar et al., 2013). Although the one-diode model is considered accurate, it is often times elaborated in order to follow the behavior of solar cells more adequately. Ben-Oretal and Appelbaum (2013) extended the set of conventional parameters in the one-diode model, to

*Corresponding author. E-mail: rachidmasrour@hotmail.com

include 8 parameters instead of 5. By adding to the model α; V_{br} and m – the cell's correction coefficient, break down voltage and exponent-power, respectively, the model was extended to cover the cell's negative-voltage operation mode, the extraction of the parameters of the single-diode solar cell model from experimental I-V characteristics of Si and Multi-junction solar cells by Appelbaum and Peled (2014). The current-voltage relationship of a diode is non-linear. The nonlinearity complicates the resolution of electrical circuits (rectifying the alternating current limiting circuit etc.). Despite this, the current-voltage (*I-V*) biased can serve as a basis for the extraction of physical parameters of ideality factor (η), series resistance (R_s) and saturation current (I_s) the knowledge precisely of these parameters allows us to understand and explain some electrical phenomena in these junctions (Mott, 1990; Sertap et al., 2010; Alivisatos, 1996). The parameters extraction requires the device and method for data analysis. A large number of published techniques (Ferhat-Hamida et al., 2002; Ortiz-Conde and García Sánchez, 2005; Zhou et al., 2009; Ranuárez et al., 2000; Lien et al., 1984; Sato and Yasumura, 1985; Cheung and Cheung, 1986; Lugo et al., 2010) describe solutions to this problem. Each of these methods has drawbacks, either in terms of use and accuracy, or at the convergence and speed (Ortiz-Conde et al., 1999). The Lambert W-function has been used in many branches of physics, especially in fractal structures (Asgarani and Mirza, 2008). The application of physics-based mixed-mode simulations to the analysis and optimization of the reverse recovery for Si-based fast recovery diodes (FREDs) using Platinum (Pt) lifetime killing is given by Cappelluti et al. (2006).

In this work, we presented two numerical methods to study the electrical behavior (I,V) of a diode. Examination of the electrical characteristic (IV) is used to extract the main parameters that characterize it, including the saturation current, series resistance and coefficient of ideality. The first method is based on the coordinates of three distinct points of the electrical characteristic (IV), to generate a system of nonlinear equations that express the electrical parameters according to the coordinates of these points and the resolution of this system non-linear equation has been performed by the digital method of Newton-Raphson. The second method developed is articulated on the least squares algorithm. The both methods are tested on the characteristic (I-V) of two diodes 1N4005 and Motorola (Ortiz-Conde et al., 2000) based on silicon, using programs developed in Matlab code. The results are discussed on the speed plan, precision and error.

Explicit analytical solutions

The equation relating the current I to the voltage V in an ideal diode is given by:

$$I = I_S\left(\exp\left(\frac{qV}{KT}\right)-1\right) \quad (1)$$

This equation is derived from the physics of semiconductors. This simplified physical model brings up a single parameter: the saturation current I_S is a leakage current flowing through the junction regardless of the type of polarization. It is due to the phenomenon of diffusion of minority carriers into the neutral areas (holes towards the p-type region and the electrons toward the n-type region) and the phenomenon of generation of free carriers in the space charge zone, q = 1.6×10^{-19}C is the electron charge, k = 1.38×10^{-38} J/K is the Boltzmann constant and T is the temperature in degrees Kelvin. A slightly more sophisticated model gives (Physics of Semiconductor Devices, 2006):

$$I = I_S\left(\exp\left(\frac{V - R_S I}{\eta V_T}\right)-1\right) \quad (2)$$

Where R_S is the series resistance, which is a parameter of major interest, the higher the value, the greater the distance from the ideal diode model. It is due to the resistance of the neutral regions of semiconductor material and making contacts ohmic semiconductor metal that can be reduced by overdoing the surface region of the semiconductor where we want to establish the ohmic contact. H is the ideality factor or quality which depends on the bias voltage. It provides information about the origin of the current flowing in the junction. It takes the value 1 if it is a diffusion mechanism. For the recombination mechanism it takes the value 2. When the two streams are similar, the factor η is a value between 1 and 2. If it takes other values, this means that other mechanisms are involved in the current transport.

Figure 1 shows the equivalent circuit for this model. It is well known that the transcendental Equation (2) cannot be solved explicitly in general *I* or *V* using common elementary functions. Therefore, it is customary to use approximate solutions explicit modeling purposes. Many of these approximate solutions have been proposed (Ortiz-Conde and Garcia Sánchez, 1992; Le Bihan, 2001) that use only the basic functions. After all, the exact explicit analytical solutions of I and V today already exist (Banwell and Jayakumar, 2000) that make use of the special function called W function Lambert of (Khalis et al., 2011), a special feature that is not expressible in terms of elementary analytic functions. W function Lambert is defined as the solution of the equation w (x) exp (w(x)) = x this function is used to solve some unsolved analytically diode. The exact analytical solution of the general equation (2) is expressed in terms of W function Lambert.

$$I = -I_S + \frac{\eta V_T}{R_S} Lambertw\left(\frac{I_S R_S}{\eta V_T}\exp\left(\frac{V + R_S I_S}{\eta V_T}\right)\right) \quad (3)$$

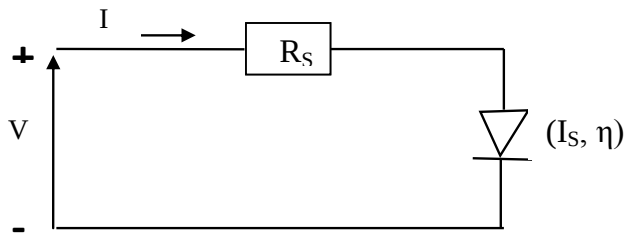

Figure 1. Equivalent circuit of a diode in a single exponential including parasitic series resistance. V_T = KT / q is the thermal voltage, *V* and *I* are the voltage and current output respectively.

METHODS

The first technique is to learn three different points of the curve, the first point to the beginning of the curve, the second just code and the third at the end. Is based on the coordinates of these points, one can generate a non-linear system of equations expressing the unknown electrical parameters *(I_s, R_S* and *η)*.

To simplify the writing of nonlinear equations (4) we take: *A(1) = I_S, A(2) = R_S* and *A(3) = ηV_T* as (V_1, I_1), (V_2, I_2) and (V_3, I_3) designate the coordinates of the three distinct points of the characteristic (I-V). While applying the Equation (2) successively to the three preceding points, one gets a system of three non linear equations therefore in three unknown A(1), A(2) and A(3):

$$\begin{cases} A(1)*(\exp((V_1\text{-}A(2)*I_1)/A(3))\text{-}1) = I_1 \\ A(1)*(\exp((V_2\text{-}A(2)*I_2)/A(3))\text{-}1) = I_2 \\ A(1)*(\exp((V_3\text{-}A(2)*I_3)/A(3))\text{-}1) = I_3 \end{cases} \quad (4)$$

To solve the system of Equations (4), we will focus on the Newton-Raphson method for solving the system of nonlinear equations. We will try to find the value A = *(A(1) A(2) A(3))*, which more or less cancel the function f = (f_1 f_2 f_3). The function f is given by Equation (5):

$$\begin{cases} f_1 = A(1)*(\exp((V_1\text{-}A(2)*I_1)/A(3))\text{-}1) - I_1 \\ f_2 = A(1)*(\exp((V_2\text{-}A(2)*I_2)/A(3))\text{-}1) - I_2 \\ f_3 = A(1)*(\exp((V_3\text{-}A(2)*I_3)/A(3))\text{-}1) - I_3 \end{cases} \quad (5)$$

The Newton-Raphson iterations can approach the value A by using the following algorithm:

$$A_k = A_{k-1} - \begin{bmatrix} \frac{\partial f_1}{\partial A(1)} & \frac{\partial f_1}{\partial A(2)} & \frac{\partial f_1}{\partial A(3)} \\ \frac{\partial f_2}{\partial A(1)} & \frac{\partial f_2}{\partial A(2)} & \frac{\partial f_2}{\partial A(3)} \\ \frac{\partial f_3}{\partial A(1)} & \frac{\partial f_3}{\partial A(2)} & \frac{\partial f_3}{\partial A(3)} \end{bmatrix}_{A_{k-1}} * f\,(A_{k-1}) \quad (6)$$

In all iterative methods, it is necessary to avoid divergence of the solution, to choose the initial value A_0. To leave not too much from one point initial x0 far from the solution.

The second method is a technique based on the least squares method (Least Mean Square LMS), this method is based on that used by S-PLUS Manual (1998) to determine the physical parameters of a solar cell. The method of least squares is one of the most widely used to model the experimental measurements by predetermined analytical function (3) methods. This method is to minimize the mean absolute or relative difference between the set of *N* measurements I_i and V_i is the result set *I* (*V_i-p*) based on the model of Equation (3). In other words, it is to minimize the following function:

$$\varepsilon = \sum_{i=1}^{N} \left(I_i - I\left(V_i, p\right)\right)^2 \quad (7)$$

Where *p = p (I_S, R_S, η)* is the set of parameters that will minimize the error ε.

RESULTS AND DISCUSSION

To validate the two proposed methods, a test was performed on the 1N4005 diode based on silicon (Lugo et al., 2010) and Motorola (Ortiz-Conde et al., 1999). The results of the characteristic measures (I-V) are shown in Figure 2.

The values of the electronic parameters found by solving nonlinear equations by the Newton-Raphson are summarized in Table 1. Substituting the average value *I_S, R_S, η* in Equation (3) of the diode characteristic and using the experimental data (I_i-V_i), one obtains the Figure 2.

From Equation (5) and from the experimental data (I_i-V_i), the principle of least squares is to minimize the function (ε) by the variation of parameters p until the deviation is minimum (where zero, if the agreement is perfect). To check if the data correctly overlay to Equation (5), the unknown electric parameters (*I_S, R_S* and *η* is plotted the two corresponding curves as shown in Figure 3. Then the Matlab output function provides). The values found by the least square method are given in Table 2.

The application of our methods to two diodes different from two different companies. The results gotten by the two technical are in good agreement with those given in

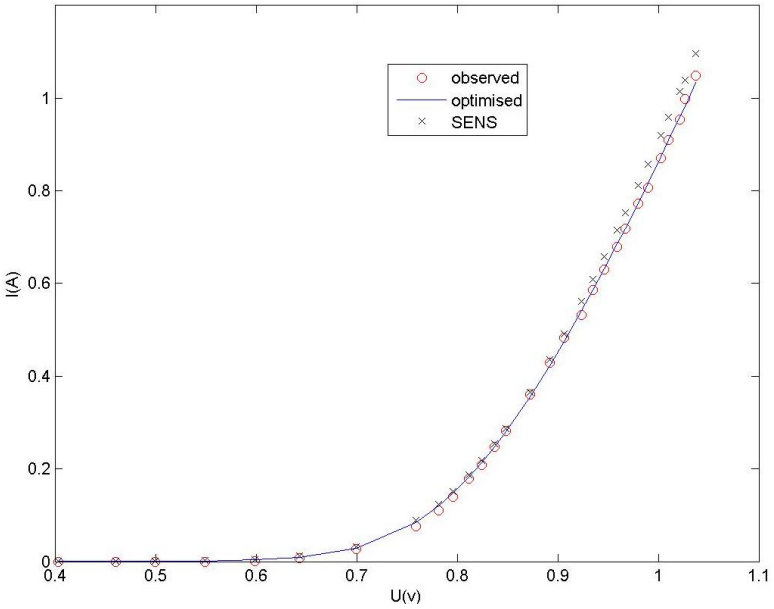

Figure 2. Comparison between the characteristic (I,V) and the method of solving the equations of nonlinear system (SENS) (Zarebski, 2007).

Table 1. Results found by the solving non-linear equations, least squares methods and Literature values for 1N4005 diode.

Parameter	Method of solving the system of nonlinear equations	Least squares method	Literature (Zarebski, 2007)
R_S (Ω)	0.14966	0.16931	0.15
I_S (nA)	31.4	11.198	4.63
H	1.95	1.815	1.7756

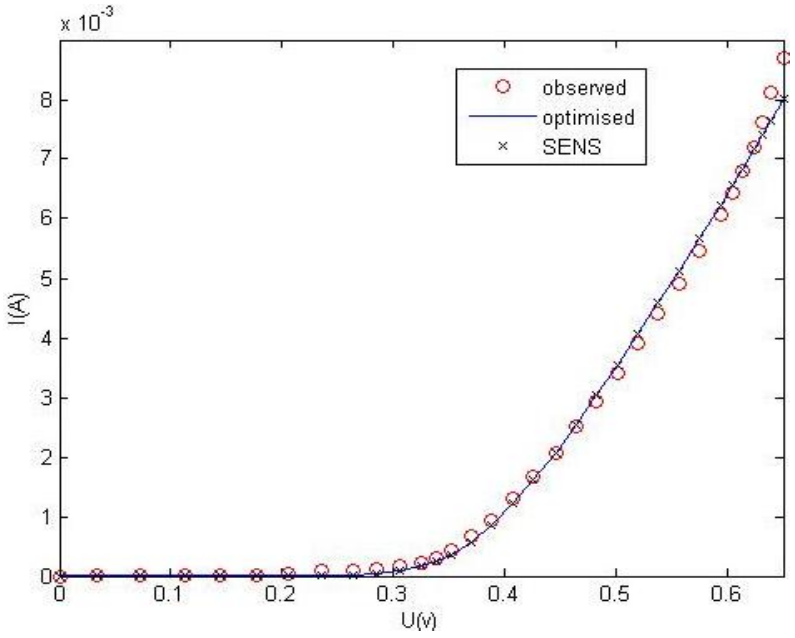

Figure 3. Comparison between the characteristic (I,V) and the method of solving the equations of nonlinear system (SENS) (Ortiz-Conde et al., 1999).

Table 2. Results found by the solving non-linear equations, least squares methods and Literature values for Motorola diode.

Parameter	Method of solving the system of nonlinear equations	Least squares method	Literature (Ortiz-Conde et al., 1999)
R_S (Ω)	27.857	28.922	33.4
I_S (nA)	0.5582	0.43968	0.58
η	0.97	0.97	1.05

the literature. It shows the hardiness of the two methods used in this work. The Newton-Raphson method converges faster in relation to least squares method.

Conclusion

In this article, we present two new methods of extracting three physical parameters of a non-ideal p-n junction from its current-voltage characteristic I = f (V). Both methods require the introduction of initial values. The first technical is method of solving the system of nonlinear equations using the some parameters given in experiment results. The second method is based on the least squares algorithm. This technical represent an extraction process of rapid and accurate parameters. The values of the physical parameters extracted by the two methods are in good agreement with the experimental values and with literature. The application of the both methods can be extended to components having same five parameters such as solar cells.

Conflict of Interest

The authors have not declared any conflict of interest.

REFERENCES

Alivisatos AP (1996). 'Semiconductor Clusters, Nanocrystals, and Quantum Dots'. Science. 271(N°5251):933–937.

Appelbaum J, Peled A (2014). Parameters extraction of solar cells - A comparative examination of three methods. Solar Energy Mater. Solar Cells. 122:164–173.

Asgarani S, Mirza B (2008). Probability distribution of (Schwämmle and Tsallis) two-parameter entropies and the Lambert W-function. Physica A. 387:6277.

Banwell TC, Jayakumar A (2000). "Exact analytical solution for the current flow through diode with series resistance. Electron Lett. 36(4):291-292.

Ben-Or A, Appelbaum J (2013). Estimation of multi-junction solar cell parameters. Progr. Photovolt. Res. Appl. 21:713–723.

Cappelluti F, Bonani F, Furno M, Ghione G, Carta R, Bellemo L, Bocchiola C, Merlin L (2006). Physics-based mixed-mode reverse recovery modeling and optimization of Si PiN and MPS fast recovery diodes. Microelectronics J. 37:190.

Cheung SK, Cheung NW (1986). 'Extraction of schottky diode parameters from forward current–voltage characteristics'. J. Appl. Phys. 49(N°2):85–87.

Chun S, Kwasinski A (2011). "Analysis of classical root-finding methods applied to digital maximum power point tracking for sustainable photovoltaic energy generation," IEEE Trans. Power Electronics. 26(12):3730–3743.

Fathabadi H (2013). Novel neural-analytical method for determining silicon/plastic solar cells and modules characteristics. Energy Convers. Manage. 76:253–259.

Ferhat-Hamida A, Ouennoughi Z, Hoffmann A, Weiss R (2002). "Extraction of Schottky diode parameters including parallel conductance using a vertical optimization method". Solid-St Electron. 46:615-619.

Hussein KH, Muta I, Hoshino T, Osakada M (1995). "Maximum photovoltaic power tracking: an algorithm for rapidly changing atmospheric conditions. Generation." IEEE Proc. Transmission Distribution 142(1):59–64.

Khalis M, Mir Y, Hemine J, Zazoui M (2011)." Extraction of equivalent circuit parameters of solar cell: influence of temperature". Eur. Phys. J. Appl. Phys. 54:10102.

Kumar G, Panchal AK (2013). A non-iterative technique for determination of solar cell parameters from the light generated IV characteristic. J. Appl. Phys. 114(8):084904.

Le Bihan J (2001). "Accurate analytical approximation for normalized diode characteristic". Theor. Appl. 29:397- 401.

Lien CD, So FCT, Nicolet MA (1984). 'An Improved Forward I–V Method for Non-Ideal Schottky Diodes with High Series Resistance'. IEEE Trans. Electron Dev. ED-31:1502-1503.

Lugo Muñoz DC, Ortiz-Conde A, García Sánchez FJ, Muci J, de Souza M, Flandre D, Pavanello MA (2010)." A cryogenic sigma-delta modulator in a standard CMOS technology " WOLTE 9-Ninth International Workshop on Low Temperature Electronics, June 21-23, Guarujá, Brazil, pp. 79 – 82.

Masoum MA, Dehbonei H, Fuchs EF (2002). "Theoretical and experimental analyses of photovoltaic systems with voltage- and current based maximum power point tracking," IEEE Trans. Energy Conver. 22(8):514–522.

Mott NF (1990). 'Metal-Insulator Transitions', Second Edition, Taylor & Francis, London, 1990.

Ortiz-Conde A, Garcia Sánchez FJ (1992). "Approximate analytical expression for equation of ideal diode with series and shunt resistances". Electron Lett. 28:1964-1965.

Ortiz-Conde A, García Sánchez FJ (2005). "Extraction of non-ideal junction model parameters from the explicit analytic solutions of its I–V characteristics," Solid-St Electron. 49:465- 472.

Ortiz-Conde A, García Sánchez FJ, Muci J (2000). "Exact analytical solutions of the forward non-ideal diode equation with series and shunt parasitic resistances." Solid-State Electron. 44:1861-1864.

Ortiz-Conde A, Ma Y, Thomson J, Santos E, Liou JJ, García Sánchez FJ, Lei M, Finol J, Layman P (1999). 'Direct extraction of semiconductor device parameters using lateral optimization method'. Solid-State Electron. 43, N°:845-848.

Physics of Semiconductor Devices, S. M. Sze. New York: Wiley, 1969, ISBN 0-471-84290-7; 2nd ed., 1981, ISBN 0-471-05661-8; 3rd ed., with Kwok K. Ng, 2006, ISBN 0-471-14323-5.

Rajasekar N, Krishna Kumar N, Venugopalan R (2013). Bacterial foraging algorithm based solar PV parameter estimation. Sol. Energy 97:255–265.

Ranuárez JC, Ortiz-Conde A, García Sánchez FJ (2000). "A new method to extract diode parameters under the presence of parasitic series and shunt resistance," Microelectronics Reliability. 40(2):355–358.

Sato K, Yasumura Y (1985). ‘Study of Forward I–V Plot for Schottky Diodes with High Series Resistance’. J. Appl. Phys. 58:3655-3657.

Sertap KA, Yakuphanoglu F, Kavasoglu N, Pakma O, Birgi O, Oktik S (2010). ‘The analysis of the charge transport mechanism of n-Si/MEH-PPV Device Structure Using Forward Bias I-V-T Characteristics’. J. Alloys. Compds. 492:421-426.

S-PLUS Manual (1998). Mathsoft Inc., Seattle, "Getting Started with S-PLUS 5.0" Washington.

Zarebski J (2007). A New Measuring Method of the Thermal Resistance of Silicon p-n Diodes. IEEE Trans. Instrumentation Measure. 56(6). December 2007.

Zhou SL, Shan Q, Fei F, Li WJ, Kwong CP, Wu PCK, Meng B, Chan CKH, Liou JYJ (2009). “Gesture recognition for interactive controllers using MEMS motion sensors,” in the 4th IEEE International Conference on Nano/Micro Engineered and Molecular Systems, *NEMS 2009,* Shenzhen. pp. 935-940.

academicJournals

Vol. 10(8), pp. 276-288, 30 April, 2015
DOI: 10.5897/IJPS2015.4288
Article Number: 4962B2A52349
ISSN 1992 - 1950

http://www.academicjournals.org/IJPS

International Journal of Physical Sciences

Full Length Research Paper

Surface and thermodynamic studies of micellization of surfactants in binary mixtures of 1,2-ethanediol and 1,2,3-propanetriol with water

Adane D. Fenta

Department of Chemistry, College of Natural and Computational Science, Arbaminch University, Arbaminch, Ethiopia.

Received 24 February, 2015; Accepted 25 March, 2015

Surface physico-chemical and thermodynamic studies of some aqueous surfactant solutions were carried out by employing conductance, surface tension and dye solubilization (UV-Vis absorption spectroscopy) techniques. From conductivity and surface tension measurements, critical micelle concentration (CMC), counter-ion association constant (α), equivalent conductance at infinite dilution (λ_o), surface exess concentration (Γ_{max}), minimum area per molecule (A_{min}), surface pressure at CMC (π_{CMC}), thermodynamic properties of micellization (ΔG^o_{mic}, ΔH^o_{mic}, ΔS^o_{mic}) and adsorption (ΔG^o_{ads}, ΔH^o_{ads}, ΔS^o_{ads}) have been obtained for an anionic (sodium dodecyl sulphate (SDS)), a cationic (hexadecyl trimethyl ammonium bromide (HTAB)) and nonionic (Polyoxyethylene (20) sorbitan mono-oleate (Tween 80)) surfactant solutions. Effect of mixing cosolvents (1,2-Ethanediol or 1,2,3-Propanetriol) on physico-chemical properties of surfactant systems at 298.15, 308.15 and 318.15K has been investigated. Surfactants micellar characteristics and their interactions with cosolvents were also investigated by Uv-vis absorption spectroscopy measurements of solutions using bromothymol blue as a probe. The inclusion of cosolvents caused an increase in CMC and degree of counterion dissociation (β) of surfactant solutions whereas the thermodynamic analysis shows that, although the micellization is less favorable in mixed solvent compared to pure water, the process is spontaneous and exothermic.

Key words: Conductance, dye solubilization, micellization, surface physico-chemical properties.

INTRODUCTION

Investigations about the micellization characteristics of different types of surfactants are still carried out mostly in water and in aqueous media containing additives that can alter the water structure. Despite extensive studies made on the micellization behavior of surfactants in different types of media, it is still not exactly clear which property of a solvent controls the micellization process. However, high cohesive energies, dielectric constants and considerable hydrogen bonding ability between the solvent molecules have been reported to be a prerequisite for aggregation of surfactants (Tharwat, 2005). In recent years there has been a renewed interest on the study of adsorption and aggregation of surfactants in solvent media containing a binary mixture of water and

E-mail: destaadane@gmail.com

a polar nonaqueous solvent as evident from published papers (Tharwat, 2005; Kabir-ud-Din and Koya, 2011; Sansanwal, 2005; Homendra and Devi, 2006; Das and Ismail, 2008; Zdziennicka, 2009; Dubey, 2008; Hideki, 2009; Zdziennicka and Jańczuk, 2010; Deepti et al., 2011; Sibani et al., 2013). Carrying out investigation on the effect of added cosolvents on the micellization of surfactants is also equally important so as to gather knowledge about the role of solvent structure on aggregation phenomenon so that it could be applied for the development of certain areas (e.g., cleaning operation, lubrication, *etc.*) which require a water-free or water-poor media (Cross and Singer, 1994; Laurier et al., 2003). Several such studies were carried out in aqueous medium and the commonly used nonelectrolytes are dimethylformamide (DMF), dimethyl sulfoxide (DMSO), dimethyl acetamide, acetonitrile, dioxane, urea and n-alkanols (Tharwat, 2005; Kabir-ud-Din and Koya, 2011; Sansanwal, 2005; Homendra and Devi, 2006; Deepti et al., 2011; Sibani et al., 2013).

1,2-Ethanediol (ED) and 1,2,3-Propanetriol(PT) are another polyhydric organic alcohols which has poly sites for hydrogen bonding and there are few reports (Hideki, 2009; Amalia et al., 2009; Nagarajan and Wang, 2000) in the literature about the micellization of ionic surfactants in water mixed medium. The author had therefore made a detailed study of the micellization behavior of an anionic (sodium dodecyl sulphate (SDS)), a cationic (hexadecyl trimethyl ammonium bromide (HTAB)) and nonionic (Polyoxyethylene (20) sorbitan mono-oleate (Tween 80)) surfactant solutions on adding the organic solvents ED or PT to water by employing conductometric, surface tension and dye solubilization (UV-Vis absorption spectroscopy) methods.

The study has been carried out at three different temperatures, 298.15, 308.15 and 318.15K, which helped to compute thermodynamic parameters of micellization assuming equilibrium model for micelle formation.

MATERIALS AND METHODS

The surfactants SDS (BDH chemicals Ltd, England), HTAB (99+%, Acros organics Ltd, USA), Tween 80 (98+%, Acros organics Ltd, USA) and organic solvents 1,2-Ethanediol (99.5%, Breckland Scientific Supplies, U.K), 1,2,3-Propanetriol(99%, Blulux, Laboratory Ltd.) were used as received. Other chemical reagents which were used in this work were: Potassium chloride (99%, Blulux, Laboratory Ltd.), Bromothymol blue (dye content: 85%, BDH chemicals Ltd, England), Absolute ethanol (99.9%, Hayman Ltd., England), n- Hexane (BDH chemicals Ltd, England), Acetone (Sigma-Aldrich, Germany), Glacial acetic acid (Hayman Ltd., England), Toluene (HPLC grade, Analytical reagent, CDH (P) LTD, India), and 1,4- Dioxane (Blulux, Laboratory Ltd.).

Conductance measurement

Conductance of ionic surfactant solutions (SDS or HTAB) with and without cosolvents(1,2-Ethanediol or 1,2,3-Propanetriol) was measured over a wide range of surfactant concentrations, at 298, 308 and 318K. The conductivity data was obtained using a digital conductivity/temp meter (ELE International, model 4071, England) equipped with a dip cell (cell constant: 1.03 cm^{-1}) and the calibration of the instrument was made with 0.01 M KCl solutions at regular time intervals and the electrode was cleaned with distilled water after each measurement. Distilled and triply deionized water with a specific conductivity of less than 1×10^{-6} Scm^{-1}, was used throughout the experiment. All the experiments were done in a thermostated water-bath holding the solution under study. The solutions (water/surfactant or water/cosolvent/surfactant mixtures) were thermally equilibrated at the desired temperature for at least 15 min before measurement. Temperature control of thermostat was within ± 0.1°C.

Surface tension measurement

Surface tension of surfactant solutions was determined by drop weight method using a specially designed stalagmometer (Wilmad lab. Glass, LG-5050-102, USA) at the desired temperatures. The stalagmometer was calibrated by determining the surface tension of pure liquids: absolute ethanol, acetone, *n*-hexane, acetic acid (glacial), toluene, 1,4-dioxane and water as standard. The observations were made in a thermostated water bath holding the solution under study. The temperature control around the solution was maintained within ± 0.1 K.

Absorbance measurement

The absorbance of surfactant solutions with and without cosolvents was measured over a wide range of surfactant concentrations, using bromothymol blue (BTB), at 298 K. Magnetically stirred (for an hour) and filtered saturated aqueous solution of BTB was used as probe for each measurement. The absorbance data was obtained using double beam UV- Visible spectrophotometer (Sanyo, SP 75, Japan) and the base line correction was made by using water (distilled and deionized). The absorbance of solutions was noted at equilibrated temperature of 25 ± 0.1°C.

RESULTS AND DISCUSSION

Critical micelle concentration

The critical micelle concentration (CMC) values of surfactants in various compositions of water-ethanediol (W/ED) and water-propanetriol (W/PT) mixtures, estimated through conductometric, surface tension and UV-Visible absorbance spectroscopy experiments at 298.15, 308.15 and 318.15K are listed in Tables 1 to 3. In these techniques, usually, CMC values are determined from the inflection point in the plots of specific conductance (κ) versus surfactant concentration (Figure 1), surface tension versus logarithm of surfactant concentration (Figure 2) and absorbance versus surfactant concentration (Figure 3) by plotting two straight lines in the pre and post micellar regions according to William's method (Tharwat, 2005; Maria et al., 2005).

In the studied pure aqueous surfactant solutions, CMC values are in the order: SDS > HTAB > Tween 80 (Tables 1 to 3). CMC of ionic surfactants (SDS or HTAB) are higher than nonionic surfactant (Tween 80) owing to the ion- ionic head group repulsion in case of the former

Table 1. Critical micelle concentration (CMC), surface excess concentration (Γ_{max}), minimum area per molecule (A_{min}) and surface pressure at CMC (π_{cmc}) for aqueous SDS solution with or without cosolvent systems.

System	T(K)	CMC (m moldm^{-3})			A	Λ_O x 10^{-1} (S cm^2 mol^{-1})	Γ_{max}×10^{10} (mol cm^{-2})	A_{min}×10^2 (nm^2)	π_{cmc} (mN m^{-1})
		*C	*S	*A					
SDS + H_2O	298.15	8.11	7.98	8.14	0.62	8.72	2.38	69.78	31.07
	308.15	8.52	8.48		0.60	9.49	2.17	76.52	31.85
	318.15	9.00	8.92		0.58	10.67	2.00	83.03	31.98
SDS + ED(1M) + H_2O	298.15	8.98	8.76	8.95	0.59	13.28	1.74	95.43	32.29
	308.15	9.23	9.17		0.55	14.95	1.66	100.0	32.84
	318.15	9.55	9.53		0.53	17.04	1.58	105.1	32.87
SDS + ED(2.5M) + H_2O	298.15	9.33	9.21	9.32	0.58	15.68	1.47	112.9	32.91
	308.15	9.40	9.29		0.56	18.03	1.41	117.7	33.26
	318.15	9.71	9.67		0.55	19.30	1.30	127.7	33.54
SDS + ED(4M) + H_2O	298.15	9.67	9.57	9.61	0.55	15.59	1.25	132.8	34.44
	308.15	9.81	9.87		0.53	17.16	1.14	145.6	34.63
	318.15	9.99	9.94		0.50	19.45	1.05	158.1	34.71
SDS + PT(1M) + H_2O	298.15	8.62	8.60	8.57	0.61	7.02	2.21	75.14	32.01
	308.15	8.88	8.86		0.58	7.85	1.99	83.45	32.39
	318.15	9.21	9.20		0.56	8.39	1.83	90.74	32.47
SDS + PT(2.5M) + H_2O	298.15	8.98	8.91	9.00	0.59	6.05	2.17	76.52	32.77
	308.15	9.18	9.06		0.58	6.46	2.03	81.80	32.99
	318.15	9.50	9.43		0.55	7.03	1.83	90.74	33.11
SDS + PT(4M) + H_2O	298.15	9.44	9.30	9.45	0.59	4.35	2.03	81.80	32.97
	308.15	9.77	9.73		0.59	4.99	1.85	89.76	33.06
	318.15	9.82	9.80		0.56	5.57	1.67	99.43	33.28

**C, *S,*A* are CMC values obtained from conductance, surface tension and absorbance measurements respectively.

surfactants (Tine and Bešter-Rogac, 2007). Lower values of CMC for HTAB in comparison to SDS is attributed to comparatively weaker ionic head groups repulsion in case of HTAB because of (a) steric hinderance of its larger sized head group and (b) deeply embedded N^+ under three methyl groups (Zdziennicka and Jańczuk, 2010).

The CMC value of an ionic surfactant solution increases on raising temperature. However, opposite trend of temperature dependence of CMC was observed in case of non ionic surfactant solutions. The positive temperature coefficient of CMC for ionic surfactants may be due to (Sansanwal, 2005; Kye et al., 2001): (a) Dehydration of surfactant ionic head groups at elevated temperature resulting in a stronger repulsion of their ionic head; and (b) Shifting of monomer ⇌ micelle equilibrium in favour of monomer at higher temperature. The negative temperature coefficient of CMC in case of non ionic surfactant is due to phase separation referred to as clouding at higher temperature.

The CMC values in pure water appear to be in good agreement with literature values (Das and Ismail, 2008; Hideki, 2009; Maria et al., 2005). On mixing ED or PT to an aqueous surfactant solution, an increase in CMC, irrespective of the nature of the surfactant, is observed (Tables 1 to 3). This may be because of lower dielectric constant of ED (ε = 36, 298.15 K) or PT (ε = 42.5, 298.15 K) as compared to water (ε = 78.36, 298.15 K). The decrease of dielectric constant (ε) of medium opposes micellization by increasing mutual repulsion of ionic heads in the micelle, hence increasing the CMC (Kabir-ud-Din and Koya, 2011;). Increase in CMC on mixing ED to a surfactant solution, being more significant compared as to PT, is due to lower dielectric constant of the former.

Counter ion association constant (α)

The post micellar and pre micellar linear plot between specific conductivity and surfactant concentration is taken equal to counter-ion dissociation constant (β). The counter-ion association constant (α) is obtained using the relation:

Table 2. Critical micelle concentration (CMC), surface excess concentration (Γ_{max}), minimum area per molecule (A_{min}) and surface pressure at CMC (π_{cmc}) for aqueous HTAB solution with or without cosolvent systems.

System	T(K)	CMC (m moldm^{-3})			A	$\Lambda_O \times 10^{-1}$ (S cm^2 mol^{-1})	$\Gamma_{max} \times 10^{10}$ (mol cm^{-2})	$A_{min} \times 10^2$ (nm^2)	π_{cmc} (mN m^{-1})
		*C	*S	*A					
HTAB + H_2O	298.15	0.92	0.88	0.90	0.77	19.49	1.78	93.29	32.23
	308.15	0.96	0.93		0.77	21.52	1.58	105.1	32.93
	318.15	1.08	0.99		0.76	24.89	1.47	112.9	32.01
HTAB + ED(1M) + H_2O	298.15	0.98	0.97	0.97	0.75	82.53	1.09	158.0	35.33
	308.15	1.09	1.06		0.72	87.65	0.96	182.5	35.72
	318.15	1.25	1.20		0.70	94.47	0.91	198.4	36.06
HTAB + ED(2.5M) + H_2O	298.15	1.26	1.23	1.22	0.68	112.4	0.90	184.5	36.27
	308.15	1.50	1.47		0.67	119.3	0.81	205.0	36.59
	318.15	1.76	1.65		0.67	124.7	0.72	230.6	36.70
HTAB + ED(4M) + H_2O	298.15	1.51	1.45	1.49	0.65	115.9	0.84	197.7	37.15
	308.15	1.73	1.65		0.64	119.1	0.75	221.4	37.40
	318.15	1.97	1.90		0.62	123.4	0.67	247.8	37.68
HTAB + PT(1M) + H_2O	298.15	0.95	0.94	0.95	0.76	21.30	1.47	112.9	34.65
	308.15	1.01	1.00		0.73	24.18	1.33	124.8	34.80
	318.15	1.15	1.08		0.71	28.04	1.19	139.5	34.95
HTAB + PT(2.5M) + H_2O	298.15	1.02	1.00	0.99	0.66	19.98	1.31	126.7	35.08
	308.15	1.21	1.14		0.66	21.88	1.16	143.1	35.69
	318.15	1.49	1.45		0.71	24.82	1.03	161.2	35.50
HTAB + PT(4M) + H_2O	298.15	1.29	1.27	1.32	0.64	17.40	1.19	139.5	36.07
	308.15	1.67	1.60		0.63	20.92	1.08	153.7	36.41
	318.15	1.81	1.76		0.64	24.31	0.97	171.2	36.75

*C, *S,*A are CMC values obtained from conductance, surface tension and absorbance measurements respectively.

$$\alpha = 1 - \beta \quad (1)$$

Counter-ion association values, as can be seen from Tables 1 and 2, for HTAB + H_2O system are higher than that of SDS + H_2O. At a fixed temperature, the α values roughly decreased with the cosolvent composition. An increase in α with respect to solvent composition is expected due to the decrease in the polarity of the bulk phase caused by the addition of cosolvents. That is, in order to diminish the repulsion between the ionic head groups, thus more fractions of the counterions would prefer to stay at the micellar surface (Kallol and Baghel, 2008; Amalia et al., 2009). However, the opposite trend obtained could be due to decrease in average aggregation number (number of molecules present in a micelle) by the addition of cosolvents, which results in a diminution of the electrostatic repulsion (that overcomes the effect of polarity changes) and leads to a diminution in the electrical charge density at the micellar surface.

With the increase in temperature, the α values of ionic surfactants in water and water–cosolvent mixtures are decreased. However, the effects of organic cosolvents on other systems were not always regular, although in some cases, a rough disorder can be seen (Zdziennicka and Jańczuk, 2010; Sarah et al., 2006).

Equivalent conductance at infinite dilution (Λ_o)

Equivalent conductance (Λ) of surfactant solutions were calculated as:

$$\Lambda = \frac{1000 \times k}{C} \quad (2)$$

Where, k is specific conductance and C is concentration in g equ/dm^3. Equivalent conductance at infinite dilution Λ_o was obtained using Onsager equation (Dubey, 2008; Tine and Bešter-Rogac, 2007):

$$\Lambda = \Lambda_o - (A\Lambda_o + B)\sqrt{C} \quad (3)$$

Where A and B are constants that explain ion- ion and

Table 3. Critical micelle concentration (CMC), surface excess concentration (Γ_{max}), minimum area per molecule (A_{min}) and surface pressure at CMC (π_{cmc}) for aqueous Tween 80 solution with or without cosolvent systems.

System	T(K)	CMC (m moldm^{-3})			A	$\Lambda_O \times 10^{-1}$ (S cm^2 mol^{-1})	$\Gamma_{max} \times 10^{10}$ (mol cm^{-2})	$A_{min} \times 10^2$ (nm^2)	π_{cmc} (mN m^{-1})
		*C	*S	*A					
Tween 80 + H_2O	298.15		0.018	0.020			1.91	86.94	19.55
	308.15		0.017				1.83	90.74	20.23
	318.15		0.015				1.82	91.24	20.62
Tween 80 + ED(1M) + H_2O	298.15		0.028	0.031			1.90	87.39	26.22
	308.15		0.025				1.85	89.76	26.56
	318.15		0.022				1.83	90.74	27.10
Tween 80 + ED(2.5M) + H_2O	298.15		0.034	0.035			1.80	92.25	29.98
	308.15		0.032				1.70	97.68	30.22
	318.15		0.030				1.60	103.8	30.77
Tween 80 + ED(4M) + H_2O	298.15		0.038	0.040			1.78	93.29	32.85
	308.15		0.035				1.68	98.84	32.95
	318.15		0.034				1.58	105.1	33.15
Tween 80 + PT(1M) + H_2O	298.15		0.025	0.028			1.89	73.15	24.21
	308.15		0.023				1.85	75.82	24.75
	318.15		0.019				1.84	77.59	25.51
Tween 80 + PT(2.5M) + H_2O	298.15		0.031	0.033			1.79	75.82	25.54
	308.15		0.030				1.74	81.40	26.70
	318.15		0.026				1.71	82.61	27.77
Tween 80 + PT(4M) + H_2O	298.15		0.034	0.037			1.73	74.46	28.14
	308.15		0.031				1.70	77.23	28.58
	318.15		0.029				1.68	80.61	29.59

*S,*A are CMC values obtained from surface tension and absorbance measurements respectively.

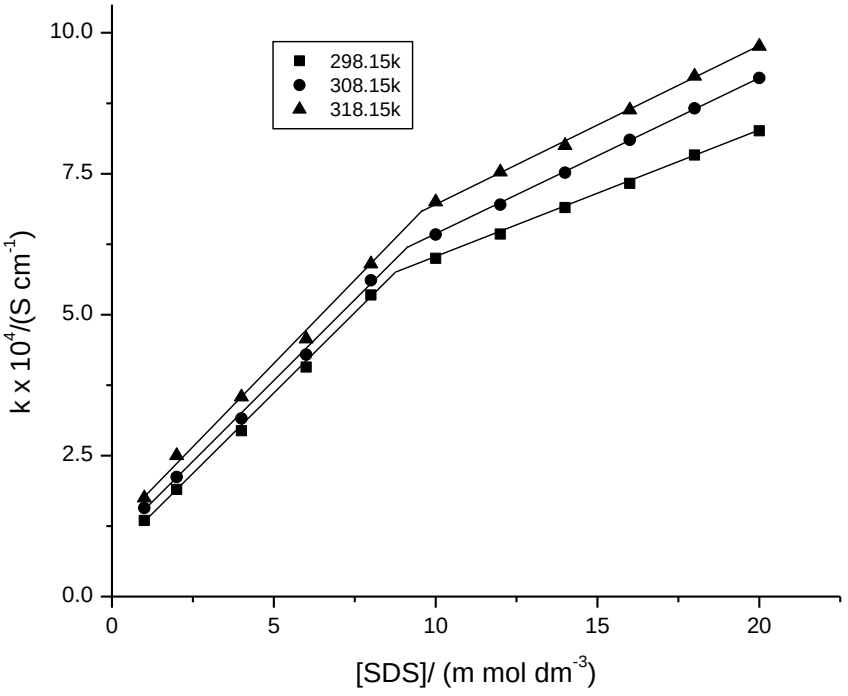

Figure 1. Plots of specific conductance (*k*) vs [SDS] for the system SDS + ED (1 M) + H_2O.

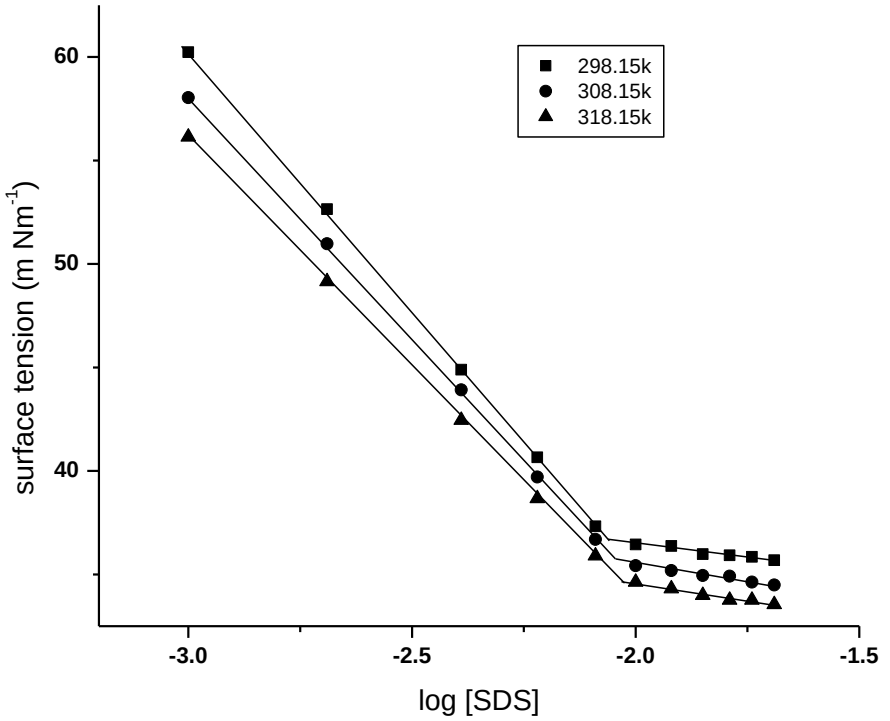

Figure 2. Plots of surface tension (γ) Vs log [SDS] for the system SDS + PT (1M) + H_2O.

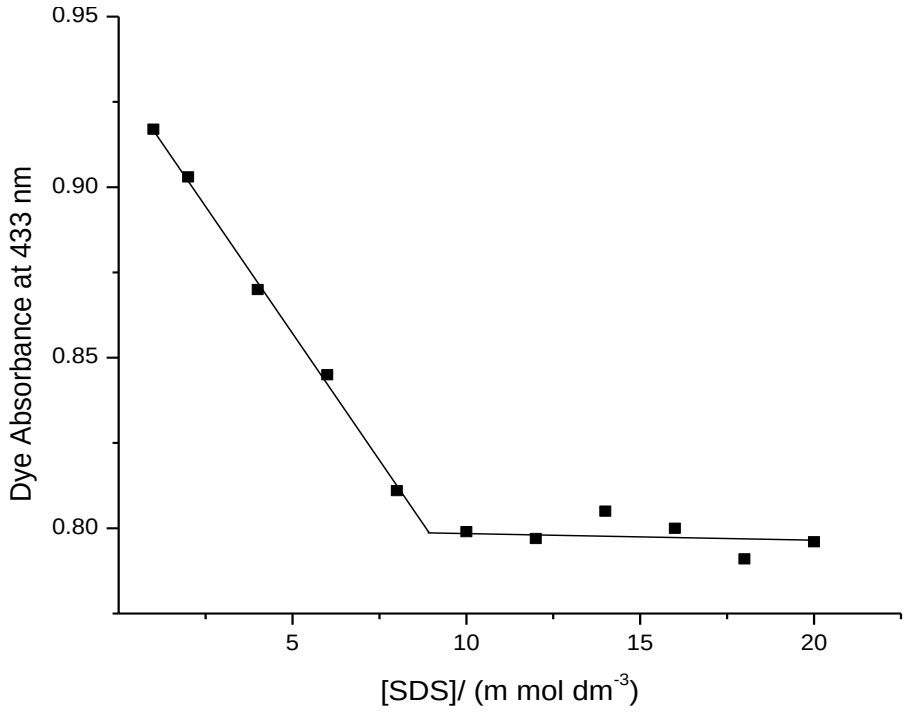

Figure 3. Plots of absorbance (*A*) Vs [SDS] for the system SDS + BTB (saturated) + ED (1 M) + H_2O, at 298.15K.

ion- solvent interaction parameters. It can be seen that (Tables 1 and 2) the observed positive temperature dependence of Λ_o values for ionic surfactant solutions is due to the increase of ionic mobility at higher

temperature. The Λ_o values for SDS + H_2O system are lower than for HTAB + H_2O system, because of higher degree of hydration of comparatively smaller head group as well as smaller counter- ion of SDS molecule compared to HTAB. The Λ_o values slightly increase on adding ED for the surfactant systems, but the reverse is true for the case of PT that may be due to enhanced intermolecular hydrogen bonding of the later with water and thus make the water structure more viscous and lower Λ_o (Yuksel, 2003; Radhouane et al., 2008).

Surface physico-chemical properties

Maximum surface excess concentration (Γ_{max}) values at the air-liquid interface has been obtained using Gibb's adsorption equation (Huang et al., 1998; Partap and Yadav, 2008):

$$\Gamma_{max} = -\frac{1}{2.303nRT}\left(\frac{d\gamma}{d\log C}\right)_T \quad (4)$$

Where *n* is the number of particles furnished by each molecule of the surfactant in the solution. Since SDS and HTAB behave as univalent electrolytes in aqueous solutions, therefore, for these surfactants the values *n* has been taken as 2.

For nonionic surfactants n=1, *R* is the gas constant. $\left(\frac{d\gamma}{d\log C}\right)_T$ represents the slope of the surface tension versus log *C* plot below the CMC at temperature *T*. The calculated values for Γ_{max} for the studied systems at three temperatures are also presented in Tables 1 to 3. It may be seen that the Γ_{max} values decrease with the increase in temperature which may be due to the enhanced molecular thermal agitation at higher temperature (Partap and Yadav, 2008).

These results are in conformity with results reported elsewhere (Yuksel, 2003; Islam and Kato, 2003). A further decrease in Γ_{max} values on mixing ED or PT may be due to the fact that addition of these cosolvents cause a partial displacement of surfactant molecules from the air-liquid interface to the bulk phase.

The minimum area per molecule (A_{min}) of surfactant at the liquid-air interface (in nm^2) was calculated using the relation (Huang et al., 1998; Partap and Yadav, 2008):

$$A_{min} = \frac{10^{14}}{N\Gamma_{max}} \quad (5)$$

Where, *N* is Avogadro's number. A_{min} values for the studied systems are also given in the Tables 1 to 3, and for binary systems the values are in the order: HTAB > Tween 80 > SDS. An examination of these values reveals that A_{min} increases both with the increase in temperature as well as with the concentration of ED and PT in the surfactant solution. This behavior can be explained in terms of the enhanced compatibility of surfactant with the solvent in the presence of cosolvents, thereby, causing a shift of surfactant molecules from air-liquid interface to the bulk phase (Kallol and Baghel, 2008; Sharma et al., 1996).

Surface pressure at CMC (π_{cmc}), an index of surface tension reduction at CMC, has been calculated using the equation (Tharwat, 2005; Yuksel, 2003):

$$\pi_{CMC} = \gamma_O - \gamma_{CMC} \quad (6)$$

Where γ_0 = surface tension of water and γ_{cmc} = surface tension of surfactant solution at CMC. π_{CMC} values thus calculated for various systems are recorded in Tables 1 to 3. An examination of the Tables clearly shows that π_{CMC} values for the studied systems vary in the order: HTAB > SDS > Tween 80. A similar order has been observed for the counter ion association constant (α) values for the former two. The surface pressure at CMC values are found to increase on adding a cosolvent for the studied ternary systems. This may be ascribed to the tendency of these organic cosolvents to adsorb at the air-liquid interface thereby lowering surface tension and hence increased π_{CMC} (Sansanwal, 2005). Further, π_{CMC} show marginal increase with increase in temperature.

Thermodynamic properties of micellization

Phase-separation and mass-action approaches present two models which have got wide acceptance for the interpretation of the energetics of micellization. For the ionic surfactants, however, the mass-action approach is usually preferred (Goodwin, 2004) and various thermodynamic parameters may be deduced from the temperature dependence of the CMC values. According to mass action model, the standard Gibbs free energy of micellization ($\Delta G°_{mic}$) for ionic and nonionic surfactant solutions were calculated using equations 3.7 and 3.8 respectively (Tharwat, 2005; Shaw, 1992).

$$\Delta G^o_{mic} = (2-\beta)RT\ln X_{CMC} \quad (7)$$

$$\Delta G^o_{mic} = RT\ln X_{CMC} \quad (8)$$

Where, β is counter-ion dissociation constant, *x* is the surfactant mole fraction at CMC and *R* is gas constant (8.314 $JK^{-1}mol^{-1}$). The corresponding entropy and enthalpy of micellization were calculated from the following expressions respectively:

$$\Delta S^o_{mic} = \left[-\frac{d(\Delta G^o_{mic})}{dT}\right]_p \quad (9)$$

$$\Delta H^o_{mic} = \Delta G^o_{mic} + T\Delta S^o_{mic} \quad (10)$$

Table 4. Thermodynamic parameters of the micellization and adsorption for SDS system in aqueous and aqueous - cosolvent environment.

System	T(k)	$-\Delta G^0_{mic}$ (kJ mol^{-1})	ΔG^0_{trans} (kJ mol^{-1})	ΔH^0_{mic} (kJ mol^{-1})	ΔS^0_{mic} (kJ mol^{-1}K^{-1})	$-\Delta G^0_{ads}$ (kJ mol^{-1})	ΔH^0_{ads} (kJ mol^{-1})	ΔS^0_{ads}(kJ mol^{-1}K^{-1})
	298.15	35.46	-	-20.25		36.78	-17.40	
SDS + H_2O	308.15	35.99	-	-20.27	0.051	37.46	-17.39	0.065
	318.15	36.47	-	-20.34		38.07	-17.39	
	298.15	34.40	1.06	-24.26		36.25	-22.54	
SDS + ED(1M) + H_2O	308.15	34.56	1.43	-24.28	0.034	36.53	-22.36	0.046
	318.15	35.08	1.39	-24.36		37.16	-22.33	
	298.15	34.05	1.41	-12.88		36.21	-23.99	
SDS + ED(2.5M) + H_2O	308.15	34.48	1.51	-12.60	0.071	36.84	-23.96	0.041
	318.15	35.46	1.01	-12.87		37.03	-23.92	
	298.15	33.26	2.20	-21.93		36.01	-24.48	
SDS + ED(4M) + H_2O	308.15	33.87	2.12	-22.16	0.038	36.80	-24.47	0.040
	318.15	34.21	2.26	-22.22		37.01	-24.28	
	298.15	35.00	0.46	-21.68		36.45	-18.56	
SDS + PT(1M) + H_2O	308.15	35.38	0.61	-21.82	0.044	37.01	-18.52	0.060
	318.15	35.87	0.60	-21.87		37.64	-18.51	
	298.15	34.40	1.06	-20.69		36.91	-27.67	
SDS + PT(2.5M) + H_2O	308.15	35.65	0.34	-21.48	0.046	37.27	-27.72	0.031
	318.15	35.71	0.76	-21.58		37.52	-27.56	
	298.15	34.02	1.44	-21.50		36.71	-22.70	
SDS + PT(4M) + H_2O	308.15	35.21	0.78	-22.28	0.042	37.00	-22.52	0.047
	318.15	35.65	0.82	-22.29		37.64	-22.49	

Further, the Gibbs energy of transfer values (ΔG^0_{trans}), which can be accounted for the effect of cosolvent on the micellization process, was estimated through (Kabir-ud-Din and Koya, 2011; Sharma et al., 1996):

$$\Delta G^o_{tras} = \Delta G^o_{mic(w-cos)} - \Delta G^o_{mic(w)} \quad (11)$$

Where, $\Delta G^o_{mic(w)}$ and $\Delta G^o_{mic(w-cos)}$ stands for standard Gibbs free energy of micellization in water and water-cosolvent mixed media, respectively.

Various thermodynamic parameters of micellization calculated using Equations (7) to (11) are presented in Tables 4 to 6. The ΔG^o_{mic} values in all the cases are negative and become less negative with the increase in the cosolvent content in the mixed media. At a fixed solvent composition, the values become slightly more negative with the rise in temperature. These values show that the micellization of surfactants in water- cosolvent (ED or PT) mixed media becomes less favorable when the solvent medium contains a higher amount of ED or PT, whereas an increase in temperature slightly favors the micellization.

According to the theory of surfactant aggregation, proposed by Nagarajan and Wang (2000), there may be various types of energy contributions to Gibbs energy of micellization. Observed positive value of ΔG^o_{tras} indicates that, it is responsible for the delay in the micellization of surfactants in the mixed media (Nagarajan and Wang, 2000) and their value depends on the transfer Gibbs free energies from pure water and the organic solvents in addition to their mutual interaction. As the addition of ED or PT modifies the bulk phase making it more favorable than pure water for dispersion of surfactant molecules, and the transfer of the hydrophobic tail from the bulk phase to the micellar region becomes less favorable, and hence ΔG^o_{mic} value increases (becomes less negative).

The standard entropy of micellization(ΔS^o_{mic}) values (Tables 4 to 6) is positive for the studied systems suggesting that the process of micellization is favored by entropy gain (16). ΔS^o_{mic} for the studied aqueous micellar solutions are in the order: Tween 80 > HTAB >SDS. On adding ED or PT, ΔS^o_{mic} values decrease due to enhanced water structure in its presence owing to intermolecular hydrogen bonding (Homendra and Devi,

Table 5. Thermodynamic parameters of the micellization and adsorption for HTAB system in aqueous and aqueous - cosolvent environment.

System	T(k)	$-\Delta G^0_{mic}$ (kJ mol^{-1})	ΔG^0_{trans} (kJ mol^{-1})	ΔH^0_{mic} (kJ mol^{-1})	ΔS^0_{mic} (kJ mol^{-1}K^{-1})	$-\Delta G^0_{ads}$ (kJ mol^{-1})	ΔH^0_{ads} (kJ mol^{-1})	ΔS^0_{ads}(kJ mol^{-1}K^{-1})
HTAB + H_2O	298.15	48.30	-	-15.50	0.110	50.11	-11.95	0.128
	308.15	49.72	-	-15.82		51.80	-11.86	
	318.15	50.49	-	-15.89		52.66	-11.94	
HTAB + ED(1M) + H_2O	298.15	47.48	0.82	-37.94	0.032	50.84	-27.29	0.079
	308.15	47.76	1.96	-37.90		51.68	-27.24	
	318.15	48.11	2.38	-37.97		52.42	-27.19	
HTAB + ED(2.5M) + H_2O	298.15	44.53	3.77	-26.34	0.061	47.56	-28.78	0.063
	308.15	45.00	4.72	-26.40		49.52	-28.11	
	318.15	45.75	4.74	-26.44		50.83	-28.71	
HTAB + ED(4M) + H_2O	298.15	42.99	5.31	-29.28	0.046	47.41	-15.81	0.106
	308.15	43.60	6.12	-29.43		48.58	-15.80	
	318.15	43.91	6.58	-29.48		49.53	-15.81	
HTAB + PT(1M) + H_2O	298.15	47.88	0.42	-34.46	0.045	50.23	-28.17	0.074
	308.15	48.37	1.35	-34.50		50.98	-28.18	
	318.15	48.78	1.71	-34.46		51.71	-28.17	
HTAB + PT(2.5M) + H_2O	298.15	44.87	3.43	-33.84	0.037	47.57	-29.99	0.064
	308.15	45.65	4.07	-34.25		49.72	-29.99	
	318.15	47.61	2.88	-35.84		51.05	-29.69	
HTAB + PT(4M) + H_2O	298.15	43.37	4.93	-21.90	0.072	46.40	-13.60	0.110
	308.15	43.43	6.29	-21.94		47.80	-13.59	
	318.15	44.81	5.68	-21.90		48.60	-13.60	

2006). On the other hand, ΔH^o_{mic} values for the studied systems are in the order: Tween 80 > HTAB > SDS. An exothermic standard enthalpy of micellization for ionic surfactants (SDS or HTAB) suggests that like entropy effect, the enthalpy change also favors the process of micellization. Positive ΔH^o_{mic}values, owing to the hydrophobic-hydrophobic interaction of surfactant alkyl chain in the process of micellization (Partap and Yadav, 2008), was observed for nonionic surfactant (Tween 80). Further, on adding a cosolvent (PT or ED) into surfactant solutions, there is decrease in ΔH^o_{mic} irrespective of their chemical nature, again due to its intermolecular hydrogen bonding with water.

Thermodynamic properties of adsorption

The standard free energy values of adsorption (ΔG^o_{ads}) at the air- liquid interface (a measure of the free energy of transfer per mole of surfactant at unit concentration from bulk to the surface at unit pressure) were calculated using the equation (Huang et al., 1998; Holmberg et al., 2003):

$$\Delta G^o_{ads} = \Delta G^o_{mic} - 6.023 \times 10^{-1} \pi_{CMC}.A_{min} \quad (12)$$

Where, π_{CMC} is in milliNewtons per meter. Values of ΔS^o_{ads} and ΔH^o_{ads} were obtained by using the corresponding Equations (13) and (14), respectively:

$$\Delta S^o_{ads} = [-\frac{d(\Delta G^o_{ads})}{dT}] \quad (13)$$

$$\Delta H^o_{ads} = \Delta G^o_{ads} + T\Delta S^o_{ads} \quad (14)$$

The values of $\Delta G°_{ads}$, $\Delta H°_{ads}$ and $\Delta S°_{ads}$ are also presented in Tables 4 to 6. The lower ΔG^0_{ads} values compared to the corresponding $\Delta G°_{mic}$ suggests that the process of adsorption of surfactant molecules at the air-liquid interface proceeds the micellization in the bulk

Standard Gibb's free energy of adsorption values for studied binary systems are in the order: SDS > Tween 80 > HTAB. This order can be explained in terms of the order of magnitude of their intermolecular head group

Table 6. Thermodynamic parameters of the micellization and adsorption for Tween 80 system in aqueous and aqueous - cosolvent environment.

System	T(k)	$-\Delta G^0_{mic}$ (kJ mol^{-1})	ΔG^0_{trans} (kJ mol^{-1})	ΔH^0_{mic} (kJ mol^{-1})	ΔS^0_{mic} (kJ mol^{-1}K^{-1})	$-\Delta G^0_{ads}$ (kJ mol^{-1})	ΔH^0_{ads} (kJ mol^{-1})	ΔS^0_{ads}(kJ mol^{-1}K^{-1})
	298.15	37.04	-	7.09		38.06	7.56	
Tween 80 + H_2O	308.15	38.43	-	7.18	0.148	39.53	7.52	0.153
	318.15	39.99	-	7.20		41.12	7.56	
	298.15	35.94	1.1	6.70		37.42	7.60	
Tween 80 + ED(1M) + H_2O	308.15	37.44	0.99	6.63	0.143	39.04	7.49	0.151
	318.15	38.99	1.00	6.51		40.63	7.41	
	298.15	35.46	1.58	5.09		37.29	7.43	
Tween 80 + ED(2.5M) + H_2O	308.15	36.80	1.63	5.11	0.136	38.75	7.47	0.150
	318.15	38.17	1.82	5.10		40.28	7.44	
	298.15	35.18	1.84	4.47		37.19	6.64	
Tween 80 + ED(4M) + H_2O	308.15	36.57	1.86	4.41	0.133	38.71	6.59	0.147
	318.15	37.84	2.15	4.47		40.13	6.53	
	298.15	36.22	0.82	7.91		37.43	5.21	
Tween 80 + PT(1M) + H_2O	308.15	37.65	0.78	7.96	0.148	39.92	4.15	0.143
	318.15	39.37	0.62	7.72		40.70	4.80	
	298.15	35.68	1.36	7.85		36.98	9.23	
Tween 80 + PT(2.5M) + H_2O	308.15	36.97	1.46	7.99	0.146	38.42	9.14	0.155
	318.15	38.55	1.44	7.90		40.08	9.23	
	298.15	35.84	1.20	0.218		37.23	1.88	
Tween 80 + PT(4M) + H_2O	308.15	36.88	1.55	0.406	0.121	38.35	1.82	0.131
	318.15	38.26	1.73	0.436		39.84	1.84	

interaction at the air–liquid interface. Such interaction (repulsion) is highest in case of SDS. It has comparatively high degree of dissociation. Such head group interaction is least in case of HTAB due to steric hindrance of its comparatively larger head group. Addition of ED or PT leads to an increase (small negative) in ΔG^0_{ads} for the studied surfactant solutions. This may be attributed to the enhanced hydrophobic (nonpolar) character of the bulk on adding cosolvents, which facilitates solubilization (Sibani et al., 2013; Meghal and Parikh, 2009) of surfactant monomers in the bulk and decrease feasibility of micellization process.

The standard entropy of adsorption (ΔS^0_{ads}) values are invariably positive and correspondingly larger than standard entropy of micellization (ΔS^0_{mic}). This may be due to more degree of freedom of the surfactant molecules at the air-liquid interface compared to that in the cramped interior of micelle. Again, the endothermic (positive) standard enthalpy of adsorption,$\Delta H°_{ads}$ values observed for nonionic surfactant (Tween 80) may be due to the breaking of Hydrogen bonds between polyoxyethylene chain oxygen of surfactant and water molecules at the air-liquid interface (Hideki, 2009). Lastly, exothermic ΔH^0_{ads} (for ionic surfactants, SDS and HTAB) and positive $\Delta S°_{ads}$ values suggest that the adsorption at air- liquid interface is favored by energy as well as entropy effect.

Nature of BTB dye absorption spectra in micellar systems

The absorption spectra of BTB in the presence of different concentration of the studied surfactant systems are shown in Figures 4 to 6. BTB in water (absence of any surfactant) shows a wavelength maximum at 433 nm. Addition of increasing concentration of surfactants with and without cosolvents led to a continuous decrease in absorbance at 433 nm. The absorption intensity at 433 nm was decreased upon further increasing the concentrations of the surfactants at constant amount of the dye indicator. That is the micellar systems altered the characteristics of the dye indicator UV spectra.

The shift in spectra is likely due to interactions between the indicators and micelles. That indicates, in micellar systems, the dye taken up by the micelles is often

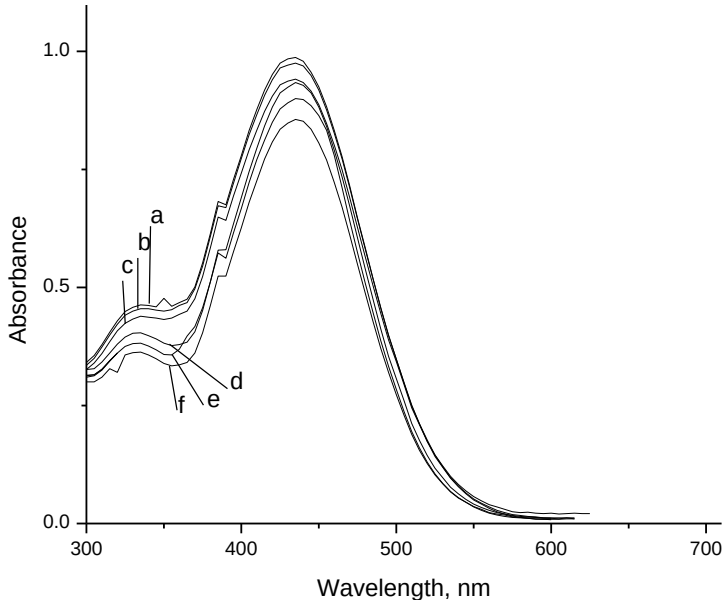

Figure 4. Absorption spectra of BTB (saturated) at various SDS concentration. [SDS]: (a) 0, (b) 0.001 M, (c) 0.005 M, (d) 0.01 M + PT (1 M), (e) 0.01 M + ED (1 M), (f) .02 M.

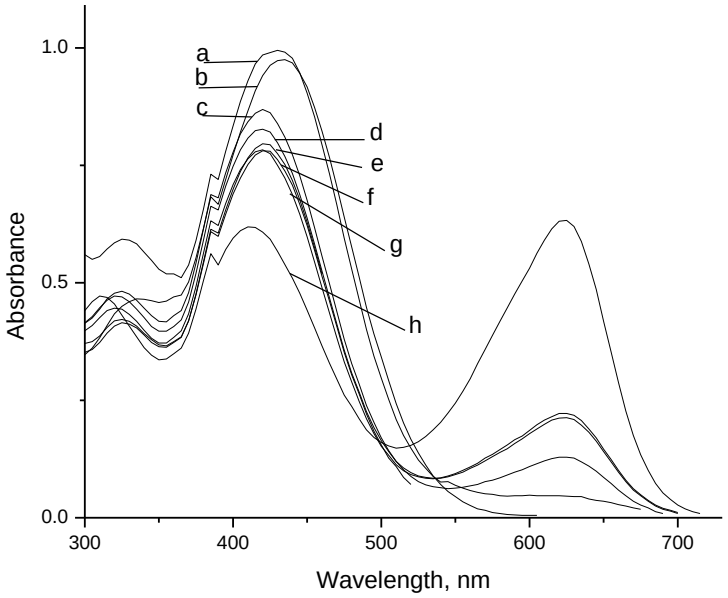

Figure 5. Absorption spectra of BTB (saturated) at various HTAB concentrations. [HTAB]: (a) 0, (b) 0.1 mM, (c) 0.5 mM, (d) 1.0 mM, (e) 1.5 mM, (f) 1.0 mM + PT (1 M), (g) 1.0 mM + ED (1M), (h) 2.8 mM.

insufficient to produce high absorbance. A similar effect of micelles on UV spectra has been reported (Jebaramya et al., 2009). In addition to that, particularly for HTAB, new peaks were appeared at 623 nm, as shown in Figure 5. Whereas absorption intensities at 623 nm are increased simultaneously with increasing the concentrations of HTAB. The development of the 623 nm band can be attributed to the conversion of the ion pair into a charge-transfer complex between the dye and micelle. Similar changes in the absorbance of the dye in the presence of oppositely charged surfactants have been reported in the past and have been attributed to the

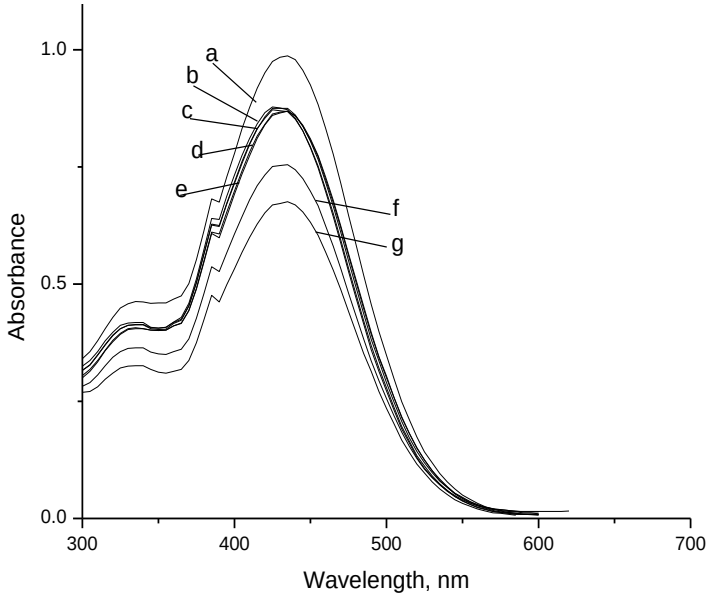

Figure 6. Absorption spectra of BTB (sat.) at various Tween 80 concentrations. [Tween 80]: (a) 0, (b) 0.005 mM, (c) 0.01 mM, (d) 0.02 mM + PT(2.5 M), (e) 0.02 mM + ED (2.5 M), (f) 0.02 Mm, (g) 0.06 mM.

formation of an ion-pair complex (Garcia et al., 2007). But as the surfactant concentration increases beyond the CMC, the absorbance of two bands (433 and 623 nm) progressively decreases with the appearance of the main dye absorption band. This indicates that the dye–surfactant complex is unstable in the micellar region, where the surfactant molecules tend to aggregate to form the micelles. The spectral changes of dye in micellar media have been suggested to be due to electrostatic interactions between oppositely charged molecules. It has been reported in the literature that the ionic dyes can form molecular complexes with oppositely charged micelles (Garcia et al., 2007). It has also been shown that aromatic compounds with sulfonic acid groups are incorporated into the Stern layer of cationic micelles in a sandwich arrangement. A van der Waals interaction between adjacent surfactant chains and the dye organic moiety (hydrophobic forces) changes the chromophore microenvironment (Jebaramya et al., 2009). The evidence that the interaction is due to oppositely charged molecules also comes from the fact that similarly charged dye-micelle systems have shown the absence of such spectral changes.

Conclusion

From the results obtained, it is possible to reach the following conclusions: Both the addition of cosolvents (ED or PT) and rise in temperature results in an increase in the critical micelle concentration (*CMC*) and degree of counterion dissociation constant (*β)* for ionic surfactants. However, CMC of Tween 80 shows a negative temperature coefficient. Again, slight increase in CMC and *β* values of studied surfactant solutions, irrespective of their chemical nature, on mixing ED was observed compared to PT. Lower ΔG^{o}_{mic} of surfactants in mixed solvent containing PT compared to that containing ED suggest more feasibility of micellization on increasing hydroxy groups in a polyol. From the observed surface properties namely surface excess concentration (Γ_{max}), minimum area per molecule (A_{min}) and surface pressure at CMC (π_{cmc}): a long chain cationic surfactant (HTAB) has relatively higher π_{cmc} and A_{min} values. On the other hand, SDS and Tween 80 have higher Γ_{max} values. Further, enhancement of π_{cmc} and A_{min} values, and reduction of Γ_{max} value have been observed in the presence of studied cosolvents. For ionic surfactant solutions, with or without a cosolvent, micellization in the bulk and adsorption at the air- liquid interface are favored by exothermic enthalpy change as well as entropy gain. And, with the increase in the concentration of cosolvents in the mixed medium, micellization becomes less favorable. Therefore, on the basis of observed effect of added cosolvents (ED and PT) on CMC, surface physico-chemical properties and thermodynamic property of the studied systems, The author suggest that, addition of these cosolvents (ED or PT) would be beneficial in metallurgical process such as concentration of ores by froth floatation and other industrial application. However, they are less effective as oil spill dispersant and in detergency process.

Conflict of Interest

The authors have not declared any conflict of interest.

ACKNOWLEDGMENTS

The author thanks Prof. O. P. Yadav and Prof. Amarendra Rajput of the Department of Chemistry, College of Natural And Computational Science, Haramaya University, Ethiopia, for their valuable suggestions during this work.

REFERENCES

Amalia R, Marı´a del Mar G, Gaspar F, Marı´a LM (2009). Effects of Glycols on the Thermodynamic and Micellar Properties of TTAB in Water. J. Colloid Interface Sci. 338:207–215.

Cross J, Singer EJ (1994). Cationic Surfactants: Analytical and Biological Evaluation. Marcel Dekker, New York.

Das D, Ismail K (2008). Aggregation and adsorption properties of sodium dodecyl sulfate in water–acetamide mixtures. J. Colloid Interface Sci. 327:198–203.

Deepti T, Kallol KG, Nadia B, Pierluigi Q, Soumen G (2011). Micellization Properties of Mixed Cationic Gemini and Cationic Monomeric Surfactants in Aqueous-Ethylene Glycol Mixture", Colloids and Surfaces A: Physicochemical and Engineering Aspects 381:61-69.

Dubey N (2008). Conductometric Study of Interaction between Sodium Dodecyl Sulfate and1-Propanol, 1-Butanol, 1-Pentanol and 1-Hexanol at Different Temperatures. J. Surface Sci. Technol. 24:139-148.

Garcia PL, Mejuto JC, Parajo M (2007). Spectroscopic and kinetic investigation of the interaction between crystal violet and sodium dodecylsulfate. J. Chem. Phy. 335:164–176.

Goodwin JW (2004). An Introduction to Colloids and Interfaces with Surfactants and Polymers. John Wiley & Sons, Ltd., west Sussex, England.

Hideki A (2009). Morphology of polysorbate 80 (Tween 80) Micelles in Aqueous 1,4-Dioxane Solutions. J. Appl. Cryst. 42:592–596.

Holmberg K, Jonsson B, Kronberg B, Lindman B (2003). Surfactants and Polymers in Aqueous Solution. 2nd edition, John Wiley & Sons, west Sussex, Chichester.

Homendra N, Devi SD (2006). Conductrometric and Surface Tension Studies on the Micellization of Some Cationic Surfactants in Water-Organic Solvent Mixed Media. J. Surface Sci. Technol. 22(3-4):89-100.

Huang JB, Mao M, Zhu BY (1998). The Surface Physico-chemical Properties of Surfactants in Ethanol–water Mixtures. J. Colloids Surfaces A: Physicochem. Eng. Aspects. 155:339–34.

Islam MN, Kato T (2003). Temperature Dependence of Surface Phase Behavior and Micelle Formation of Some Nonionic Surfactants. J. Phys. Chem. 107- 965.

Jebaramya J, Ilanchelian M, Prabahar S (2009). Spectral Studies of Toluidine Blue O in the Presence of Sodium Dodecyl Sulfate. J. Nanomaterials Biostruc. 4(4):789-797.

Kabir-ud-Din, Koya PA (2011). Effects of acetonitrile on the micellization and thermodynamic parameters of tetradecyltrimethylammonium bromide: Conductometric and fluorimetric studies/ J. Molecular Liquids doi: 10.1016/j.molliq.2010.11.003.

Kallol KG, Baghel V (2008). Micellar Properties of Benzyldimethyldodecylammonium Bromide in Aquo–organic Solvent Media. Indian J. Chem. 47A:1230-1233.

Kye HK, Kim HU, Lim KH (2001). Effect of temperature on critical micelle concentration and thermodynamic potentials of micellization of anionic ammonium dodecyl sulfate and cationic octadecyl trimethyl ammonium chloride. Colloids and Surfaces A: Physicochemical and Eng. Aspect 189:113–121.

Laurier LS, Stasiuk EN, Marangoni DG (2003). Surfactants and their applications. Annu. Rep. Prog. Chem. Sect. 99:3–48.

Maria DM, Munoz M, Rodrı´guez A, Moya ML (2005). Water-*N*,*N*-Dimethyl formamide Alkyltrimethylammonium Bromide Micellar Solutions: Thermodynamic, Structural, and Kinetic Studies. *Langmuir*, 21:3303-3310.

Meghal D, Parikh J (2009). Thermodynamic study for aggregation behavior of hydrotropic solution. World Academy Sci. Eng. Tech. 57:56-69.

Nagarajan R, Wang CC (2000). Theory of surfactant aggregation in water/glycols mixed solvents. Langmuir 16:5242-5251.

Partap R, Yadav OP (2008). Effect of Inorganic Ions on Surface Properties of Non-ionic Surfactant at Various Temperatures in Aqueous Medium. Ind. J. Chem. 47A:1524-1527.

Radhouane C, Louis CM, Charnay C, Derrien G, Zajac J (2008). Interactions of Phenol with Cationic Micelles of Hexadecyltrimethylammonium Bromide Studied by Titration Calorimetry, Conductimetry, and ^{1}H NMR in the Range of Low Additive and Surfactant Concentrations. J. Colloid Interface Sci. 326:227–234.

Sansanwal PK (2005). Effect of Co-solutes on Physicochemical Properties of Surfactant solutions. J. Sci. industrial Res. 65:57-64.

Sarah E, Moore M, Mohareb I, Stephanie AM, Palepu RM (2006). Conductometric and Fluorometric Investigations on the Mixed Micellar Systems of Cationic Surfactants in Aqueous Media. J. Colloid Interface Sci. 304(4):491–496.

Sharma VK, Yadav OP, Singh J (1996). Physico-chemical Studies of Sodium Dodecyl Sulphate Solutions in Pyridine and Isomeric Picolines. J. Colloids and Surfaces A: Physicochem. Eng. Aspects. 110:23-35.

Shaw DJ (1992). Introduction to Colloid and Surface Chemistry. 4th edition, Butterwoth-Heinemann, London.

Sibani D, Satyajit M, Soumen G (2013). Physicochemical Studies on the Micellization of Cationic, Anionic and Nonionic Surfactants in Water-Polar Organic Solvent Mixtures". J. Chem. Eng. Data. 58:2586-2595.

Tharwat FT (2005). Applied surfactants: Principles and Applications. 2nd Edition, Wokingham, United Kingdom.

Tine MP, Bešter-Rogac M (2007). Thermodynamics of Micelle Formation of Alkyltrimethylammonium Chlorides from High Performance Electric Conductivity Measurements. J. Colloid Interface *Sci.*13:288–295

Yuksel B (2003). Micelle Formation in SDS and Dodecyltrimethylammonium Bromide at Different Temperatures. Turk. J. Chem. 27:487–492.

Zdziennicka A (2009). Adsorption and Volumetric Properties of Triton X-100 and Propanol Mixtures. J. Colloid Interface Sci. 336:423–430.

Zdziennicka A, Jańczuk B (2010). Behavior of Cationic Surfactants and Short Chain Alcohols in Mixed Surface Layers at Water–air and Polymer–water Interfaces with regard to Polymer Wettability. J. Colloid Interface Sci. 349:374–383.

academicJournals

Vol. 10(8), pp. 289-305, 30 April, 2015
DOI: 10.5897/IJPS2014.4239
Article Number: 6BBA9CA52354
ISSN 1992 - 1950

http://www.academicjournals.org/IJPS

International Journal of Physical Sciences

Full Length Research Paper

Relativistic causality versus superluminal communication: Is the quantum mechanics a semi-empirical theory?

Piero Chiarelli

National Council of Research of Italy, Area of Pisa, 56124 Pisa, Moruzzi 1, Italy Interdepartmental Center "E. Piaggio" University of Pisa, Italy.

Received 26 November, 2014; Accepted 4 March, 2015

The work analyzes the compatibility between the classical freedom, the local relativistic causality and the non-local behavior of quantum mechanics in the frame of the stochastic approach of the quantum hydrodynamic analogy (SQHA). The work describes the role of the quantum potential in generating the quantum non-local dynamics in a fluctuating environment. The analysis shows that it is possible to maintain the concept of classical freedom between far away weakly bounded systems (moderate non-locality) as well as to make compatible the uncertainty principle with the relativistic postulate of invariance of light speed. The work shows that the paradox of instantaneous quantum non local behavior at infinite distances of the standard formalism is an artifact due to the non-relativistic non-stochastic ambit of such theory where the light speed is infinite and the non-local interaction owns an infinite range of action. The work envisages that the SQHA can possibly lead to a fully theoretically self-standing quantum mechanics where the wave function collapse, during a measurement process, can be described by the theory itself without empirical postulates. Under this light the paper discusses the need of searching for (both local and non-local) hidden variables quantum mechanics as well as the need of superluminal communications in quantum experiments. The analysis shows that all these hypotheses are attempts of interpreting the outputs of quantum measurements that cannot be fully explained by the semi-empirical formalism of quantum mechanics, based on the statistical postulates of the measuring process as well as the existence of a classical observer. A two photon experiment is discussed to the light of the SQHA approach.

Key words: Quantum non-locality, superluminal transmission of quantum information, classical freedom, local relativistic causality, Einstein, Podolsky, and Rosen (EPR) paradox, macroscopic quantum decoherence, Bell's inequalities, quantum hydrodynamic analogy.

INTRODUCTION

The conflict between the quantum non-locality and the local character of the classical macroscopic experience is one of the most intriguing problems of the modern physics (Schrödinger, 1935; Einstein et al., 1935; Bell, 1964; Greenberger et al., 1990).

This fact has lead to many logical paradoxes that contrast with our sense of reality (Schrödinger, 1935; Einstein et al., 1935; Bell, 1964). The most known quantitative tentative to investigate the problem is given by Bell (1964) in response to the so called EPR paradox (Einstein

et al., 1935) a critical analysis of the quantum non-locality respect to the notion of macroscopic classical freedom and local relativistic causality.

The central point of the problem is the leaking of the theoretical connection between the quantum mechanics and the classical one that would explain how the laws of physics pass from the quantum behavior to the classical one. The disconnection between the two theories leaves open the question about the hierarchy between them. The quantum mechanics, on the base of its semi-empirical statistical approach, needs the classical mechanics (that is, the classical observer) to be defined, while the quantum one seems to be the basic one from which the classical mechanics can stem out in the macroscopic limit where $\hbar$ tends to zero (Bialyniki-Birula et al., 1992).

One current of thought is represented by the "deterministic" approach to quantum mechanics that analyzes how the quantum equations are the generalization of the classical one (Bialyniki-Birula et al., 1992; Bohm, 1952; Madelung, 1926; Jánossy, 1962; Jánossy, 1962; Wyatt, 2005; Nelson, 1967, 1985; Guerra and Ruggero, 1973; Parisi and Wu, 1981) where the non-locality is introduced in various ways, the Madelung quantum potential (Bialyniki-Birula et al., 1992; Madelung, 1926; Jánossy, 1962), the Nelson's osmotic potential, the Bohm-Hylei quantum potential or the Paris and Wu fifth-time parameter.

A great help in explaining the origin of the non-locality of quantum mechanics comes from the QHA equations (Bialyniki-Birula et al., 1992; Madelung, 1926; Jánossy, 1962) that shows how the non-local restrictions come in the playing from the quantization of vortexes (Bialyniki-Birula et al., 1992) and by the elastic-like energy arising by the quantum pseudo-potential. On the contrary, the Schrödinger equation is a differential equation where the non-local character of evolution is determined by the initial and boundary conditions that must be defined for describing a physical problem and that are apart from the equation.

In the case of charged particles, the non-local properties of the Schrödinger equation come also from the presence of the electromagnetic (EM) potentials that depend by the intensities of EM fields in a non-local way (e.g., Aharonov –Bohm effect) (Wyatt, 2005). In the corresponding hydrodynamic equations (Bialyniki-Birula et al., 1992) the EM potentials do not appear but only in local way through the strength of the EM fields. The mathematically more clear origin of the quantum restrictions in the QHA make it suitable for the achievement of the connection between quantum concepts (probabilities) and classical ones (e.g., trajectories) (Wyatt, 2005) helping in overcoming the contrast between the quantum non-local behavior and our classical sense of reality.

The deterministic approach of the QHA and similar theories gains interest in the physics community due to the fact that it helps in explaining quantum phenomena that cannot be easily described by the usual formalism. They are multiple tunneling (Jona et al., 1981), critical phenomena at zero temperature (Ruggiero and Zannetti, 1981), mesoscopic physics (Ruggiero and Zannetti, 1983a, b; Chiarelli, 2013a), numerical solution of the time-dependent Schrödinger equation (Weiner and Askar, 1971; Weiner and Forman, 1974; Terlecki et al., 1982), quantum dispersive phenomena in semiconductors (Gardner, 1994), quantum field theoretical regularization procedure (Breit et al., 1984) and the quantization of Gauge fields, without gauge fixing and without ensuing the Faddeev-Popov ghost (Zwanziger, 1984).

On the theoretical point of view, one of the most promising aspect of this model is helping in investigating the quantum mechanical problems using efficient mathematical technique such as the stochastic calculus, the numerical approach and the supersymmetry.

A more recent and sophisticated approach is given by t'Hooft (1988, 1996, 1999). He proposes the obtaining of the quantum mechanics through a process of loss of information by using outputs coming from the black-hole thermodynamics and by the so called holographic principle (Susskind et al., 1993; Bousso, 2002).

A parallel current of thought, investigates the possibility of obtaining the classical state through the loss of quantum coherence in classically chaotic systems due to the presence of stochastic fluctuations (Cerruti et al., 2000; Calzetta and Hu, 1995; Wang et al., 2008; Lombardo and Villar, 2005; Mariano et al., 2001). In this case, most of the results are obtained by numerical and semi-empirical approaches, leaking of global theoretical view.

The present paper investigates the non-local property of quantum mechanics and its decoherence as a consequence of fluctuations by using the QHA (Madelung, 1926; Jánossy, 1962; Wyatt, 2005) implemented with the stochastic calculus. This strategy is supported by the advantage of the QHA in managing the non-local quantum dynamics in system larger than a single atom when fluctuations becomes important (Bousquet et al., 2001; Morato and Ugolini, 2011; Chiarelli, 2013b) and by its completeness respect to the Bohmian mechanics (Chiarelli, 2012; Bohm and Vigier, 1954).

E-mail: pchiare@ifc.cnr.it, Tel: +39-050-315-2359. Fax: +39-050-315-2166.

PACS: 03.65.Ud, 03.67.Mn, 03.65.Ta, 03.75.Gg.

Stochastic generalization of the quantum hydrodynamic analogy

The QHA-equations are based on the fact that the Schrödinger equation, applied to a wave function $\psi_{(q,t)} = |\psi|_{(q,t)} \; exp\; [\; \frac{i}{\hbar} S_{(q,t)}\;]$, is equivalent to the motion of a particle density $n_{(q,t)} = |\psi|^2_{(q,t)}$ with velocity $\dot{q} = \frac{\nabla S_{(q,t)}}{m}$ (Bialyniki-Birula et al., 1992). In presence of stochastic noise $\eta_{(q,t,T)}$, that for the sufficiently general case, to be of practical interest, can be assumed Gaussian with null correlation time, the stochastic partial differential conservation equation for $n_{(q,t)}$ reads (Chiarelli, 2013b):

$$\partial_t n_{(q,t)} = -\nabla \bullet (n_{(q,t)} \dot{q}) + \eta_{(q,t,T)} \tag{1}$$

$$< \eta_{(q_\alpha,t)}, \eta_{(q_\beta+\lambda,t+\tau)} > = < \eta_{(q_\alpha)}, \eta_{(q_\beta)} > G(\lambda)\delta(\tau)\delta_{\alpha\beta} \tag{2}$$

$$\dot{p} = -\nabla (V_{(q)} + V_{qu(n)}), \tag{3}$$

$$\dot{q} = \frac{\nabla S}{m} = \frac{p}{m}, \tag{4}$$

$$V_{qu} = -(\frac{\hbar^2}{2m}) n^{-1/2} \nabla \bullet \nabla n^{1/2}. \tag{5}$$

$$S = \int_{t_0}^{t} dt (\frac{p \bullet p}{2m} - V_{(q)} - V_{qu(n)}) \tag{6}$$

$$\lim_{T \to 0} G(\lambda) = exp[\; -(\frac{\lambda}{\lambda_c})^2\;]. \tag{7}$$

where T is the noise amplitude parameter (e.g., the temperature of an ideal gas thermostat put in equilibrium with the system (Chiarelli, 2013b) and $G(\lambda)$ is the shape of the spatial correlation function of η.

The noise spatial correlation function (7), is a direct consequence of the derivatives present into the quantum potential that give rise to an elastic-like contribution to the system energy that reads (Weiner, 1983):

$$\overline{H}_{qu} = \int_{-\infty}^{\infty} n_{(q,t)} V_{qu(q,t)} dq = -\int_{-\infty}^{\infty} n_{(q,t)}^{1/2} (\frac{\hbar^2}{2m}) \nabla \bullet \nabla n_{(q,t)}^{1/2} dq \tag{8}$$

where a large "curvature" of $n_{(q,t)}$ leads to high quantum potential energy. This can be easily checked by calculating the quantum potential of the wave function $\psi = cos\; \frac{2\pi}{\lambda} q$ that reads:

$$V_{qu} = -(\frac{\hbar^2}{2m}) \left(cos^2 \frac{2\pi}{\lambda} q\right)^{-1/2} \nabla \bullet \nabla \left(cos^2 \frac{2\pi}{\lambda} q\right)^{1/2} = \frac{\hbar^2}{2m} \left(\frac{2\pi}{\lambda}\right)^2 \tag{9}$$

Showing that the energy increases as the inverse squared of the distance λ between two adjacent peaks (that is, the wave length). In the stochastic case, given Gaussian fluctuations with correlation distance λ, (9) represents the energy of the frequency mode associated to the closest independent fluctuations.

Therefore, independent fluctuations of particle density (PD) very close each other (that is, $\lambda \to 0$), generating very high curvature on the density $n_{(q,t)}$, can lead to a whatever large quantum potential energy even in the case of vanishing fluctuations amplitude (that is, $T \to 0$).

In this case, fluctuations with infinitesimal amplitude (that is, $T \to 0$) and diverging energy content, can lead to a finite quantum potential energy contribution even in the limit of T=0 forbidding the convergence of equations (1-7) to the deterministic limit (Bialyniki-Birula et al., 1992) (that is, the standard quantum mechanics).

Therefore, in order to eliminating these unphysical solutions, the additional conditions (7) come into the set of the equations leading to physically coherent stochastic generalization of quantum mechanics (Chiarelli, 2013b).

If we require that $\overline{H}_{qu} < \infty$ (following the criterion that higher is the energy lower is the probability to reach the corresponding state (that is, state with infinite energy have zero probability to realize itself) it follows that independent fluctuations of the density $n_{(q,t)}$ on shorter and shorter distance are progressively suppressed (that is, have lower and lower probability of happening). This physical effect due to the quantum potential (that confers to the particle density function the elastic behavior like a membrane, very rigid against short range curvature) imposes a finite correlation length to the possible physical fluctuations.

In the small noise limit (Chiarelli, 2013b) the suppression of PD fluctuations on very short distance, due to the finite energy requirement, brings to a restriction on the correlation length of the noise itself λ_c in (7) (Chiarelli, 2013b) that reads:

$$\lim_{T \to 0} \lambda_c = 2 \frac{\hbar}{(2mkT)^{1/2}}, \tag{10}$$

leading to explicit form of the variance (2) (Chiarelli, 2013b).

$$\lim_{T\to 0} <\eta_{(q_\alpha,t)},\eta_{(q_\beta+\lambda,t+\tau)}>= \mu\frac{kT}{2\lambda_c{}^2}exp[-(\frac{\lambda}{\lambda_c})^2]\delta(\tau)\delta_{\alpha\beta} \quad (11)$$

Where μ is a constant with the dimension of a migration coefficient.

Furthermore, in the case of very small noise amplitude, due to the constraints (11), the action (6), can be re-cast in the form (Chiarelli, 2013b):

$$\begin{aligned} S &= \int_{t_0}^{t} dt(\frac{p\bullet p}{2m} - V_{(q)} - V_{qu(n)}) \\ &= \int_{t_0}^{t} dt(\frac{p\bullet p}{2m} - V_{(q)} - V_{qu(n_0)} - \delta V_{qu}), \\ &= S_0 + \delta S \end{aligned} \quad (12)$$

Where δS is a vanishing small fluctuating quantity (Chiarelli, 2013b).

Non-local property of quantum potential in presence of noise

The quantized action depends by the values of the quantum potential related to the corresponding eigenstates (that is, stationary states). On the other hand, the eigen values are determined by the quantum potential that has to neutralize the force deriving by the Hamiltonian potential (Appendix A). Since this condition must happen in all points of the space the dynamics of a generic quantum state is clearly non-local.

If we consider a bi-dimensional space, the quantum potential makes the particle density function acting like an elastic membrane that becomes quite rigid against ripples with very short wave length.

Given that the force of the quantum potential in a point depends by the state of the system around it, it introduces the non-local character into the motion equations. For this reason, the quantum non-local properties can be very well identified and studied by means of the analytical mathematical investigations of the property of the quantum potential in Equation (5).

In order to analytically detail what happens in the macroscopic case, mathematically speaking, we observe that the quantum force (equal to minus the gradient of the quantum potential) cannot be taken out by the deterministic limit of Equation (1) as intuitively proposed by many authors (Bialyniki-Birula et al., 1992; Weiner, 1983) because this operation will wipe out the quantum stationary states (that is, quantum eigenstates) deeply changing the structure of such equation.

The presence of the QP is needed for the realization of the quantum eigenstates that happen when the force of the QP exactly balances the Hamiltonian one. On the contrary, in the stochastic case, when we deal with large-scale systems with physical length $\mathcal{L} >> \lambda_c$ submitted to fluctuations, in weakly interacting systems we can have a vanishing small quantum force at large distances (Appendix B) (Chiarelli, 2013a, b) that, becoming much smaller than fluctuations, can be correctly neglected in the motion equations.

It must be underlined that not all types of interactions lead to a vanishing small quantum force at large distance (a straightforward example is given by linear systems where the quantum potential owns a quadratic form (Appendix B, sections B.1-B.2) (Chiarelli, 2013a, b, c, d).

Nevertheless, there exists a large number of non-linear long-range weak potentials (e.g., Lennard Jones types) where the quantum potential tends to zero (Appendix B) at infinity and can be neglected (Chiarelli, 2013c). In this case a rarefied gas of such particles having the mean particle distance much larger that the quantum potential range of interaction (Chiarelli, 2013a, b) behaves as a classical phase.

Following we analyze the large scale form of the SPDE (1) for asymptotically vanishing quantum potential with finite range of interaction λ_q (24, B.5).

In order to investigate this point, let's consider a system whose Hamiltonian which reads:

$$H = \frac{p^2}{2m} + V_{(q)}, \quad (13)$$

in this case the QHA equations (Bialyniki-Birula et al., 1992;) (that is, the deterministic limit of (17)) can be derived by the following phase-space equation:

$$\partial_t \rho_{(q,p,t)} + \nabla\bullet(\rho_{(q,p,t)}(\dot{x}_H + \dot{x}_{qu})) = 0 \quad (14)$$

Where

$$n_{(q,t)} = \iiint \rho_{(q,p,t)} d^{3n}p. \quad (15)$$

$$\dot{x}_H = (\partial_p H, -\nabla H) \quad (16)$$

$$\dot{x}_{qu} = (0, -\nabla V_{qu}) \quad (17)$$

by integrating equation (14) over the momentum p with the conditions that $\lim_{|p|\to\infty} \rho_{(q,p,t)} = 0$, with the constraint on the quantum phase space density ρ (a Wigner-like function):

$$\rho_{(q,p,t)} = n_{(q,t)}\,\delta(p - \nabla S). \quad (18)$$

The factor $\delta(p-\nabla S)$ warrants the wave-particle equivalence

in the quantum mechanics limit and the correspondence rule:

$$p = m\dot{q} = \nabla S \tag{19}$$

between the quantum hydrodynamic model and the Schrödinger equation (Bialyniki-Birula et al., 1992; Weiner, 1983).

When a spatially distributed random noise is present, Equation (17) has the corresponding phase space SPDE that reads

$$\partial_t \rho_{(q,p,t)} + \nabla \bullet (\rho_{(q,p,t)} (\dot{x}_H + \dot{x}_{qu})) = \eta_{(q,t,T)} \delta (p - \nabla S), \tag{20}$$

whose zero noise limit is the deterministic PDE (14). Near the deterministic limit, in the case of Gaussian noise (2), it is possible to re-cast (20) as:

$$\partial_t \rho_{(q,pt)} + \nabla \bullet (\rho_{(q,pt)} (\dot{x}_H + \dot{x}_{qu(\rho_0)})) = -\nabla \bullet (\rho_{(q,pt)} \delta \dot{x}_{qu}) + \eta_{(q,t,T)} \delta (p - \nabla S), \tag{21}$$

where ρ_0 is the solution of the deterministic QHA equations and where $\delta \dot{x}_{qu} = (0, -\nabla \delta V_{qu})$, where:

$$\begin{aligned} \delta V_{qu} &= -(\frac{\hbar^2}{2m}) \{ \mathrm{n}^{-1/2} \nabla \bullet \nabla \mathrm{n}^{1/2} - \mathrm{n}_0{}^{-1/2} \nabla \bullet \nabla \mathrm{n}_0{}^{1/2} \}. \\ &= V_{qu(\mathrm{n})} - V_{qu(\mathrm{n}_0)} \end{aligned} \tag{22}$$

where $\mathrm{n}_{0(q,t)} = \iiint \rho_{0(q,p,t)} d^{3n} p$.

Thanks to conditions (7, 10) (Chiarelli, 2013b), closer and closer we get to the deterministic limit (that is, $\frac{\lambda_c}{\mathcal{L}} \to \infty$, where $\mathcal{L}$ is the physical length of the system), smaller and smaller is the amplitude of the random term on the right side of (21):

$$-\nabla \bullet (\rho_{(q,p,t)} \delta \dot{x}_{qu}) + \eta_{(q,t,T)} \delta (p - \nabla S) = X_{(q,t)} \tag{23}$$

When $\frac{\lambda_c}{\mathcal{L}} \to \infty$ the standard quantum mechanics is achieved and the quantum potential cannot be disregarded from the hydrodynamic quantum motion equations.

Large-scale classical behavior in non-linear asymptotically weakly-bonded systems

On the contrary, when $\lambda_c << \mathcal{L}$, in weakly bounded system when the force steaming from the quantum potential at large distance tends to zero it is possible to coherently define a measure of the quantum potential range of interaction λ_q that reads (Chiarelli, 2013b):

$$\lambda_q = 2\lambda_c \frac{\int_0^{\infty} | q^{-1} \frac{\partial V_{qu}}{\partial q} | dq}{| \frac{\partial V_{qu}}{\partial q} |_{(q=\lambda_c)}}, \tag{24}$$

When $\lambda_q < k \in \Re$ the quantum potential becomes much smaller than its fluctuations at large distance ad it can correctly be disregarded by the equation of motion.

Thence, when $\frac{\lambda_q}{\mathcal{L}} \to 0$ it follows that:

$$\dot{x}_{qu(\rho_0)} << \delta \dot{x}_{qu} \tag{25}$$

Where Equation (25) expresses the fact that the quantum potential force $\dot{x}_{qu(\rho_0)} = (0, -\nabla V_{qu(\rho_0)})$ is much smaller than its fluctuations $\delta \dot{x}_{qu(\rho_0)} = (0, -\nabla \delta V_{qu})$ (that is, $| \nabla V_{qu(\mathrm{n}_0)} | << | \nabla \delta V_{qu(\mathrm{n})} |$).

For sake of completeness, we observe that close to the deterministic limit (that is, to the quantum mechanics) when $\mathcal{L} < \lambda_c$ the quantum potential cannot be disregarded even if it is vanishing small, therefore the quantum potential range of interaction λ_q is physically meaningful if, and only if, $\lambda_q > \lambda_c$. For $\lambda_q < \lambda_c$ the quantum potential range of interaction must be retained equal to λ_c.

Introducing (25) into equation (21), for $\mathcal{L} >> \lambda_q \geq \lambda_c$, it follows that:

$$\partial_t \rho_{(q,p,t)} + \nabla \bullet (\rho_{(q,p,t)} (\dot{x}_H)) \cong -\nabla \bullet (\rho_{(q,p,t)} \delta \dot{x}_{qu}) + \eta_{(q,t,T)} \delta (p - \nabla S) \tag{26}$$

and that

$$\lim_{\frac{\lambda_c}{\mathcal{L}} \to 0} < \eta_{(q_\alpha,t)}, \eta_{(q_\beta + \lambda, t+\tau)} >= \mu (\frac{kT}{2m})^{\frac{1}{2}} \delta(\lambda) \delta(\tau) \delta_{\alpha\beta} \tag{27}$$

Given that for $\mathcal{L} >> \lambda_q \geq \lambda_c$ the noise amplitude results $T >> T_c = \frac{\hbar^2}{2mk\mathcal{L}^2}$ (where for $\mathcal{L} = 3 \times 10^{-6}$ cm and m

equal to the proton mass T_C can be as low as 3°K) in weakly bounded with system $\lambda_q \approx \lambda_c$ (Chiarelli, 2013a) the stochastic phase space PDE (26) reads:

$$\partial_t \rho_{(q,p,t)} + \nabla \bullet (\rho_{(q,p,t)} (\dot{x}_H)) = X_{(q,t)}. \quad (28)$$

where $X_{(q,t)}$ is a stochastic (sufficiently small quantity) giving rise to classically fluctuating dynamics that do not own eigenstates.

Physically speaking, the central point in weakly quantum entangled systems, whose characteristic length $\mathcal{L}$ is much bigger than the quantum potential range of interaction λ_q, is that the stochastic sequence of fluctuations of the quantum potential does not allow the coherent reconstruction of the superposition of state since they are much bigger than the quantum potential itself. In this case (especially in classically chaotic systems) the effect of the quantum potential with fluctuations on the dynamics of the system is not equal to the effect of its average (even in the unlikely case of fluctuations have a null time mean).

If the quantum potential can be disregarded in the large scale description, the action (12) reads:

$$\begin{aligned} S &= \int_{t_0}^{t} dt \left(\frac{p \bullet p}{2m} - V_{(q)} - V_{qu(n_0)} - \delta V_{qu} \right) \\ &\cong \int_{t_0}^{t} dt \left(\frac{p \bullet p}{2m} - V_{(q)} - \delta V_{qu} \right) \\ &= S_{cl} + \delta S \end{aligned} \quad (29)$$

and hence, the momentum of the solutions given by the δ-function in Equation (18) (that is, $\delta (p - \nabla (S_{cl} + \delta S))$ approaches the classical value (plus a fluctuation) and reads:

$$p = \nabla (S_{cl} + \delta S) = p_{cl} + \delta p \quad (30)$$

Observing that the quantum coherence length λ_C results by the geometrical mean of the stochastic length $\frac{\hbar c}{kT}$ (of order of unity or less, (about 1,44 cm at 1°K)) and the Compton length $l_C = \frac{\hbar}{mc}$ (the reference length for the standard quantum mechanics) it follows that the description of a macroscopic system (with a resolution Δq such as $\lambda_c, l_C, \lambda_q < \Delta q << \mathcal{L}$) can behave classically stochastic at laboratory scale, even at low temperature, since for T_C as small as the temperature of the background radiation 2,725°K, it results $\lambda_c \propto (\frac{l_C \hbar c}{kT})^{1/2} = 2.8 x 10^{-8} m$ for a particle of proton mass (or $\lambda_c \approx 3 x 10^{-9} m$ at a temperature of 300°K)).

Even if the condition $\lambda_c < \lambda_q < \Delta q$ is usually satisfied for macroscopic objects constituted by Lennard-Jones interacting particles, there also exists (at laboratory condition) the possibility to have $\Delta q < \lambda_q$ and, hence, to detect quantum phenomena.

The most direct and immediate example is given by observables depending by molecular properties of solid crystals that, due to the linearity of the particles interaction, can own a very large quantum potential range of action λ_q (that may result of order of ten times of the atomic distances (Chiarelli, 2013a).

Another possibility is to refrigerate a fluid below its critical density (if it does not undergo solidification) in order to obtain that the mean molecular distance becomes smaller than λ_p or/and λ_c (Chiarelli, 2013b).

Even if the linear systems are the most studied and known ones, those characterized by non-linear weak interactions, to which equation (28) can apply, are more wide-spread in nature.

For instance, equation (28) can apply to the case of a rarefied gas phase of Lennard-Jones potential interacting particles where the mean inter-particle distance d is much bigger than λ_q and λ_c (for instance for the helium at room temperature it results $\lambda_c \approx \lambda_q \approx 0.6 x 10^{-8} cm$ and $d \approx 6 x 10^{-7} cm$). In this case, the quantum superposition of states of molecules (or group of them) does not exist so that the macroscopic gas system behaves classically.

A deeper analysis (Chiarelli, 2013a), shows that the classical behavior of molecules of a real gas is maintained down to the density of liquids. On the contrary, due to the linearity of intermolecular forces in solid crystals, λ_q becomes bigger than the mean inter-particle distance (Chiarelli, 2013a) and the quantum behavior of groups of atoms is maintained. Nevertheless, since the linear interaction of solids ends over a certain distance, the quantum behavior survives just in phenomena depending by the molecular scale (e.g., Bragg's diffraction).

The quantum macroscopic state of a body made of weakly interacting particles like ordinary molecules does not have any physical existence in a noisy environment.

COMPATIBILITY BETWEEN THE LOCAL RELATIVISTIC CAUSALITY AND THE (NON-LOCAL) QUANTUM UNCERTAINTY RELATIONS IN THE FRAME OF THE SQHA

If in the classical macroscopic reality we try to detect

microscopic variables, below a certain point the wave-particle dual properties of bodies emerge thanks to the quantum potential effect. In the classical approach the particle concept owns the characteristic that position and velocity are perceived as independent. On the other hand, on microscopic scale the wave property of the matter (e.g., the impossibility to interact just with a part of the system without entirely perturbing it) leads to the coupling between conjugated variables such as position and velocity (Oppenheim and Wehner, 2007). If we increase of spatial confinement of the wave function, an increase of the quantum potential energy (due to the overall increase of derivatives of $n^{1/2}$) is produced. This fact leads to possible higher particle momentum values in the following measurements.

The scale-dependence of the quantum potential interaction leads the classical perception of the reality until the resolution size Δq is at least larger than the quantum coherence length λ_c.

Moreover, we observe that higher is the amplitude of the noise T, smaller is the length λ_c and, hence, higher is the attainable degree of spatial precision within the classical scale. On the other hand, higher is the amplitude of noise, higher are the fluctuations of observables such as the velocity and/or energy. In the frame of the SQHA, it is straightforward to show that these mutual opposite effects on conjugated variables are the basis of the Heisenberg principle of uncertainty. In fact, by using the quantum stochastic hydrodynamic model, it is possible to derive the relation between the time interval Δt of a measurement and the related variance of the energy on a particle of mass *m*.

If on distances smaller than λ_c any system behave in quantum mode (as a wave) so that any its sub-parts cannot be perturbed without disturbing all the entire system, it follows that the independence between the measuring apparatus and the measured system (*classical freedom*) requires that they must be far apart, at least, more than $\frac{\lambda_c}{2}$ and hence for the finite speed of propagation of interactions and information (*local relativistic causality* (LRC)) the measure process must last longer than the time $\tau = \frac{\lambda_c}{c}$.

Moreover, given that the noise $\eta_{(q,t,T)}$ in (13) in the small noise limit (that is, T sufficiently small) leads to Gaussian energy fluctuations (Chiarelli, 2013b), it follows that the mean value of the energy fluctuation for each degree of freedom of a particle is $\Delta E_{(T)} = \frac{1}{2}kT$ (Ozawa, 2003) and thence, in the non-relativistic limit ($mc^2 >> kT$) for a particle of mass *m*, the energy variance ΔE reads:

$$\Delta E \approx (<(mc^2+\Delta E_{(T)})^2-(mc^2)^2>)^{1/2} \cong (<(mc^2)^2+2\Delta E_{(T)}-(mc^2)^2>)^{1/2} \cong (2mc^2<\Delta E_{(T)}>)^{1/2} \cong (2mc^2kT)^{1/2} \quad (31)$$

from which it follows that (Chiarelli, 2013b; Ozawa, 2003)

$$\Delta E \Delta t > \Delta E \Delta \tau = \frac{(2mc^2kT)^{1/2}\lambda_c}{2c} = \hbar \cdot \quad (32)$$

It is worth noting that the product $\Delta E \Delta \tau$ is constant since the growing of the energy variance with the square root of the temperature $\Delta E \approx (2mc^2kT)^{1/2}$ is exactly compensated by the decrease of the minimum time of measurement:

$$\tau \propto \frac{\hbar}{(2mc^2kT)^{1/2}} \quad (33)$$

furnishing an elegant physical explanation why the Heisenberg relations exist in term of a physical constant.

The same result is achieved if we derive the uncertainty relation between the position and the momentum of a particle of mass *m*.

If we measure the spatial position of a particle with a precision of $2\Delta L > \lambda_c$ so that we do not perturb its quantum wave function (that, due to environmental fluctuations, is spontaneously localized on a spatial domain of order of λ_c) the variance Δp of the modulus of its relativistic momentum $(p^\mu p_\mu)^{1/2} = mc$ due to the vacuum fluctuations reads:

$$\Delta p \approx (<(mc+\frac{\Delta E_{(T)}}{c})^2-(mc)^2>)^{1/2} \cong (<(mc)^2+2m\Delta E_{(T)}-(mc)^2>)^{1/2} \cong (2m<\Delta E_{(T)}>)^{1/2} \cong (2mkT)^{1/2} \quad (34)$$

leading to the uncertainty relationship

$$\Delta L \Delta p > \frac{\lambda_c}{2}\Delta p = \frac{\lambda_c}{2}(2mkT)^{1/2} = \hbar \quad (35)$$

If we impose measuring the spatial position with a precision $2\Delta L < \lambda_c$, we have to localize the quantum state of the particle more than what is spontaneously is.

Since quantum potential realizes the particle-wave equivalence, the wave-function localization and momentum variance are submitted to the properties of the Fourier transform relationships (holding for any wave system): The uncertainty relations remain satisfied anyway we try to localize the wave function (either by

environmental fluctuations or by physical means (that is, external potentials).

Connections between the uncertainty relations and local relativistic causality

In the frame of the SQHA, particles are necessarily correlated each other until they are separated by a distance smaller than λ_c, the distance over which the wave function is governed by quantum law (they still may present quantum correlations (stochastic influenced) until they are separated by a distance up to λ_q, but in this case we do not have quantum entanglement as described by the standard (deterministic) quantum mechanics).

If two particles are quantum entangled, when the measurement on one of the two is performed (so that the global wave-function collapses to an eigenstate) in the context of the SQHA model, we are in presence of a kinetic (irreversible) evolution toward a stationary state (eigenstate) (SQE) with its characteristic (not null) time τ_c.

If we assume the Copenhagen interpretation of quantum mechanics, so that the measurement process ends when the wave function is collapsed to the eigenstate, the "quantum relaxation" interval of time τ_c represents the minimum time of measurement. In this case, the compatibility of the SQHA (that is, of the quantum mechanics) with the *local relativistic causality* implies that it must be $\tau_c > \tau = \frac{\lambda_c}{c}$ (or at least $\tau_c > \frac{\lambda_c}{2c}$ if the wave function decoherence starts from the center toward the border).

From experimental point of view, in order to demonstrate that the *local relativistic causality* (LRC) breaks down in quantum processes, it needs to demonstrated that the decoherence time τ_c is so short that the wave function collapse to the eigenstate is faster than the light to travel the radius $\frac{\lambda_c}{2}$ over which the quantum entangled state extends itself and hence, it is sufficient to demonstrate that $\tau_c < \frac{\lambda_c}{2c}$.

Given that, by introducing (10) in (31) in presence of environmental energy fluctuations it holds:

$$\lambda_c = \frac{2\hbar c}{\Delta E} \tag{36}$$

and hence $\Delta E \tau_c < \hbar$, it follows that, in the SQHA model (that is, low speed limit), the violation of the Heisenberg uncertainty principle necessarily involves the LRC breaking and (for microscopic systems with characteristic length $\mathcal{L} < \lambda_c$) vice versa.

The same conclusion is achieved if, by using external means, we confine the wave function in a region of length $\Delta L < \lambda_c$.

RELATIVISTIC APPROACH

The SQHA approach is the classical limit of the corresponding relativistic model. In such low velocity limit model, the light speed goes to infinity and hence the compatibility with the RLC can be checked just showing that the uncertainty relations are compatible with the requirement of finite speed of interactions.

Even if the stochastic generalization of the quantum relativistic hydrodynamic approach is still not available, from the hydrodynamic representation of the Dirac equation (Chiarelli, 2014a) we can inspect the Lorentz invariance of the relativistic quantum potential that can enforce the hypothesis of compatibility between the LRC and the quantum non-locality. The relativistic quantum potential allows verifying if the non-local interactions that it introduces into the quantum equation of motion propagate themselves compatibly with the postulate of the relativity about the invariance of light speed as the fastest way to which signals and interactions can be transmitted.

Since the invariance of light speed is the generating property of the Lorentz transformations, the co-variant form (that is, invariant 4-scalar product) of quantum potential that reads (Chiarelli, 2014b):

$$V_{qu} = -\frac{\hbar}{2i}\left[\overset{\bullet}{q}^{\mu} \partial_{\mu} ln[\frac{\boldsymbol{R}}{\overline{\boldsymbol{R}}}] \right] \tag{37}$$

where

$$ln[\frac{\boldsymbol{R}}{\overline{\boldsymbol{R}}}] = \left(ln[\frac{|\Psi_1|}{|\Psi_3|}],\ ln[\frac{|\Psi_2|}{|\Psi_4|}],\ ln[\frac{|\Psi_3|}{|\Psi_1|}],\ ln[\frac{|\Psi_4|}{|\Psi_2|}] \right) \tag{38}$$

$$\overset{\bullet}{q}^{\mu} = \frac{\overline{\Psi} c \gamma^{\mu} \Psi}{|\Psi|^2} = \frac{\Psi * c \gamma^0 \gamma^{\mu} \Psi}{|\Psi|^2} \tag{39}$$

where Ψ_i are the components of the bispinor 4-dimensional wave function

$$\Psi = (\Psi_1, \Psi_2, \Psi_3, \Psi_4),$$

and where γ^{μ} are the 4x4 matrices derived by the 2x2

Pauli matrices (Bialyniki-Birula et al., 1992), united to the property of the 4-dimensional wave function Ψ that changes accordingly with the Lorentz transformation, allows affirming that the quantum non-local behavior (deriving by the quantum potential) is compatible with such a postulate of the relativity.

In fact, whatever inertial system we choose moving with velocity $v < c$, the quantum potential expression (37) describes the quantum dynamics as realize themselves in such new reference system (where the light speed is always c and hence not attainable). This fact forbids that in any inertial system the time difference between the initial conditions (e.g., starting of measurement (that is, cause)) and the final one (wave collapse (that is, effect)) is null (or negative) so that the quantum-potential action on the whole wave function cannot realize itself in a null time.

This result enforces the hypothesis that any measurable quantum non-local process (even involving a large distance) is compatible with the postulate of invariance of light speed as the fastest way to which signals and interactions can be transmitted.

The paradox of instantaneous non local quantum action at infinite distances is, hence, an artifact that appears in the non-relativistic non-stochastic theories of quantum mechanics due to the fact that the light speed tends to infinity and the non-local interaction own an infinite range of action.

COMMENTS ABOUT THE SQHA MODEL

In the frame of the stochastic QHA the achievement of the classical characteristics of physical reality (Einstein et al., 1935) such as the classical freedom and local relativistic causality is realized as a large-scale effect in systems of asymptotically weakly bounded particles.

As far as the resolution limit of the classical description is much larger than the length over which the wave (quantum) properties of the matter can be detected, the classical concepts are not contradicted. When we deal with observables of microscopic systems, the quantum properties arise since the quantum potential (that is, the wave property of the matter) comes into effect.

The SQHA shows that the *classical freedom* principle (independence between systems) and the local relativistic causality are compatible with the quantum mechanics in the frame of a unique theory.

The possibility of *classical freedom* comes from the fact that, in fluctuating environment asymptotically weakly bounded systems can disentangle themselves at large distance (beyond the quantum coherence lengths λ_c and quantum potential range of action λ_q).

It also noteworthy that in the frame of the SQHA model, linear system (or more tightly bounded ones) do not disentangle themselves even at large distance forbidding the realization of the large-scale classical behavior (so that the classical universe as we know is a direct consequence of the electrical and gravitational forces that goes to zero at infinity).

The recovering of the quantum mechanics as the deterministic limit of a stochastic theory (that is, the SQHA) fulfills the philosophical need of determinism (Schrödinger, 1935; Einstein et al., 1935; Bell, 1964). In the SQHA model the quantum mechanics represent the deterministic limit of a stochastic theory. In this picture, the deterministic quantum distribution functions can be thought as a sort of “mechanical-like” distributions (not statistical) whose evolution is determined and well defined once the initial distributions and boundary conditions are defined.

The statistical variability and hence the indeterminism of the system evolution is introduced by the environmental fluctuations.

In the context of the SQHA model, the large-scale classical freedom allows the realization of statistical measurements so that, in principle, the description of the measurement process (as the interaction with a classical observer system) can find its description inside the theory itself.

In the SQHA, the wave-function collapse to an eigenstate (due to the interaction with a large scale apparatus in a classical fluctuating environment) can descend by the irreversible dynamics of the stochastic motion equations as a kinetic process to a stationary state (eigenstate).

This fact leads to a quantum theory with the conceptual property of a complete theory (that does not need additional postulates) able to describe the quantum evolution even during irreversible quantum processes such as the measurements.

In the frame of the SQHA model, a non-local based theory with the property of large scale *local freedom* compatible with the relativistic postulate of maximum speed of light and information transmission (*local relativistic causality*) has no necessity to postulate superluminal transmission of information to explain the result of quantum experiments obtained at large distance.

To this end, in the final part of this work we want to examine the logical consequences of assuming the existence of superluminal transmission of information in quantum experiments.

ARE SUPERLUMINAL INFORMATION EXCHANGED DURING QUANTUM EXPERIMENTS?

The attempts of solving the problem of quantum correlations between experiments at large distance (that dates back to the foundation of the quantum physics) have followed various ways: The local treatment of quantum mechanics possibly with the help of hidden

(local) variables. This possibility has been shown to be not realizable by the violation of Bell's inequalities (Bell, 1964).

The establishing of non-local theory compatible with the classical physics: The completion of quantum mechanics by using non-local hidden variables. This hypothesis argues that the fully quantum evolution is determined by information that cannot be obtained by the observer (von Neumann, 1932/1955). The Bohmian mechanics furnishes an example of this completion where the hidden variables are non local (Maudlin, 1994).

The assumption that there is a sort of quantum kinetic synchronization among quantum entangled particles that is maintained along irreversible processes (such as the measurement ones) happening in presence of fluctuations and involving large-scale classical objects. This point of view basically hypothesizes that exists a more general quantum theory able to comprehend the classical, relativistic and irreversible phenomena. Superluminal information are exchanged during quantum measurements.

The cases 2A and 2B even similar, differ each other: the first one considers that the quantum mechanics is a complete theory for describing the system evolution but it has a leaking of information about additional (non-local) variables that the classical observer cannot achieve; the second one is based upon the assumption that the theoretical quantum equations themselves do not allow the complete description of the evolution.

The latter hypothesis can be justified by fact that the standard quantum mechanics is a semi-empirical theory (needing additional empirical postulates) that is not able to describe the quantum irreversible evolution of the wave function collapse to an eigenstate during a measure.

On the other hand, if the decay to an eigenstate cannot be determined by the quantum motion equation, but only in a probabilistic way, generally speaking, this means that we do not have all the complete "machinery" to describe the quantum evolution of a system.

About the existence of superluminal communications in quantum experiments, Clauser Horne, Shimony and Holt (CHSH) (Clauser et al., 1969) have shown that in quantum mechanics experiments the Tirelson's limit of the correlation coefficient $S_{CHSH} = 2\sqrt{2}$ cannot be overcame, while Popescu and Rohrlich (Popescu and Rohrlich, 1994) showed that superluminal communication is not necessary for correlated experiments with $S_{CHSH} \leq 4$ and hence, in principle, they may be not needed in quantum mechanics.

In order to analyze the problem under the light of the SQHA model, we discuss below the output of a two entangled photons experiment traveling in opposite direction in the state:

$$|\psi>= \frac{1}{\sqrt{2}}|H,H> + e^{i\phi}|V,V> \quad (40)$$

that cross polarizers oriented in the same direction following the scheme in Figure 1.

The assumption that the state of the photon is defined only after the measurement has taken place leads to accept that the photon superposition state interacts with the polarizer, but it is still not fully collapsed neither to $|H>$ nor to $|V>$ until it is adsorbed by the polarizer or by the photon counter.

Given that in the SQHA approach the wave function collapse is not instantaneous (but takes a time interval that we name Δt_1 and Δt_2 for the two photons, respectively), the measurement time τ_m starts at the arrival of the first entangled photon at its polarizer-photon counter system (at the time t_1) and ends when the other entangled one is detected at the second polarizer-photon counter system (at the time $t_2 = t_1 + \tau_m$) (the contemporary detection of the photons at the two photon-counters systems when placed at the same distance from the source for instance, does not imply that the duration of the measurement process is null).

The better way to perform the experiment is to increase as much as possible the distance between the two polarizer-photon counter systems $\mathcal{L}$. The best possibility is to have such a distance that spans over a cosmological length. To comply with this condition, we can think to have the source on the Earth, one polarizer-photon counter system on the Moon and the other on Mars. We can also suppose that the Moon, the Earth and the Mars are aligned each others. In this case , it follows that the distance between the two polarizer-photon counter systems $\mathcal{L} = \mathcal{D}_{e\text{-}mo} + \mathcal{D}_{e\text{-}ma}$ and that $t_1 = \frac{\mathcal{D}_{e\text{-}mo}}{c}$, $t_2 = \frac{\mathcal{D}_{e\text{-}mo}}{c} + \tau_m$, where $\mathcal{D}_{e\text{-}mo} \cong 3{,}84\ x10^8\ m$ and $\mathcal{D}_{e\text{-}ma}$ are the Earth-Moon and the Earth-Mars distances respectively.

If we assume that the quantum potential (QP) propagates itself at the speed of light for bringing the information about the first photon detection to the second one, it follows that the measurement time lasts longer than $\tau_m = \Delta t_1 + \Delta t_2 + \frac{\mathcal{L}}{c}$.

Thence, the time delay Δt between the arrival of the second photon to mars and its detection must result:

$$\Delta t = t_2 - \frac{\mathcal{D}_{e\text{-}ma}}{c} = \frac{\mathcal{D}_{e\text{-}mo}}{c} + \tau_m - \frac{\mathcal{D}_{e\text{-}ma}}{c} = 2\frac{\mathcal{D}_{e\text{-}mo}}{c} + \Delta t_1 + \Delta t_2 \quad (41)$$

Thence if $\Delta t < 2\frac{\mathcal{D}_{e\text{-}mo}}{c} + \Delta t_1 + \Delta t_2$ or better, $\Delta t < 2\frac{\mathcal{D}_{e\text{-}mo}}{c} \cong 2.55\,s$ (and, hence, $\tau_m < \frac{\mathcal{L}}{c}$) the photon

wave function collapse on mars has happened before the arrival of the quantum potential signal coming from the first photon detection on the Moon. In this case there is no possibility of transferring quantum information between the two photons without violating the RLC. Therefore two alternative possibilities remain:

1. Superluminal transmission of information during the experiment, and
2. Intrinsic dynamical synchronization fully describeable via a complete relativistic quantum stochastic theory.

The two possibilities exclude themselves each other: if we own the complete quantum model we would be able to describe any physical event without additional hypotheses. On the other hand if we do not have it, we need a surrogate hypothesis, to fill the gap that in this case consists in hypothesizing the superluminal transmission of information. In this case, we have to define the kind and the characteristics of such an interaction and its "mechanics" since it is not contained in the quantum one.

Conclusion

The work analyzes the non-local property of quantum mechanics in the frame of the stochastic QHA model and shows that it can have a finite range of action, allowing in weakly bounded systems the realization of the classical mechanics on large scale limit.

The analysis shows that it is possible to maintain the concept of *freedom* of the classical reality between far away systems beyond the range of interaction of quantum potential as well as to make compatible the *local relativistic causality* with the uncertainty principle, one of the most relevant manifestations of the non-local behavior of the quantum mechanics.

The *moderate non-locality* of the SQHA approach can be compatible with the assumption that the speed of light is the maximum velocity of transmission of information and interactions. This is confirmed by the relativistic QHA approach that shows that the quantum potential propagates the non-local quantum interaction accordingly with the relativistic postulate of light speed invariance as the maximum velocity of transmission.

The model shows that the paradox of instantaneous quantum action at infinite distances is an artifact that appears in the non-relativistic non-stochastic limit of quantum mechanics where the light speed goes to infinity and non-locality becomes a global property.

The SQHA model shows that is possible to have a theory where *moderate non-locality*, *classical freedom* and *relativistic causality* can cohabit together showing that there is no need for searching a local quantum mechanics (giving a theoretical support to the Bell's inequality violations).

On the base of a simple two photon experiment, the paper shows that the intellectual necessity of postulating that superluminal information are exchanged during non-local quantum experiments may be due to the leaking of theoretical completeness of the standard quantum formalism.

REFERENCES

Bell JS (1964). On the Einstain-Podolsky-Rosen paradox". Physics. 1:195-200.

Bialyniki-Birula I, Cieplak M, Kaminski J (1992). "Theory of Quanta". Oxford University press, Ny. 87-111, 369-381.

Bohm D (1952). A suggested interpretation of quantum theory in terms of "hidden" variables. Phys Rev. 85:166,180.

Bohm D, Vigier JP (1954). Model of the causal interpretation of quantum theory in terms of a fluid with irregular fluctuations. Phys. Rev. 96:208-216.

Bousquet D, Hughes KH, Micha DA, Burghardt I (2001). Extended hydrodynamic approach to quantum-classical nonequilibrium evolution I. Theory. J. Chem. Phys. P. 134.

Bousso R (2002). The holographic principle. Rev. Mod Phys. 74:825.

Breit JD, Gupta S, Zaks A (1984). Stochastic quantization and regularization. Nucl. Phys. B. 233:61.

Calzetta E, Hu BL (1995). Quantum Fluctuations, Decoherence of the Mean Field, and Structure Formation in the Early Universe. Phys. Rev. D. 52:6770-6788.

Cerruti NR, Lakshminarayan A, Lefebvre TH, Tomsovic S (2000). Exploring phase space localization of chaotic eigenstates via parametric variation. Phys. Rev. E 63:016208.

Chiarelli P (2012). Is the quantum hydrodynamic analogy more general than the Schrödinger approach? Intell. Arch. 1(2):21.

Chiarelli P (2013a). The classical mechanics from the quantum equation. Phys. Rew. Res. Int. 3(1):1-**9.**

Chiarelli P (2013b). The uncertainty principle derived by the finite transmission speed of light and information. J. Adv. Phys. 2013; 3:257-266.

Chiarelli P (2013c). Quantum to classical transition in the stochastic hydrodynamic analogy: The explanation of the Lindemann relation and the analogies between the maximum of density at lambda point and that at the water-ice phase transition. Phys. Rev. Res. Int. 3(4): 348-366.

Chiarelli P (2013d). Can fluctuating quantum states acquire the classical behavior on large scale? J. Adv. Phys. 2:139-163.

Chiarelli P (2014a) .The quantum hydrodynamic formulation of Dirac equation and its generalized stochastic and non-linear analogs, accepted for publication to Phys. In Press.

Chiarelli P (2014b). The quantum potential: the missing interaction in the density maximum of He^4 at the lambda point? Am. J. Phys. Chem. 2(6):122-131.

Clauser JF, Horne MA, Shimony A, Holt RA (1969). Proposed experiment to test local hidden-variable theories". Phys. Rev. Lett. 23(15):880–884.

Einstein A, Podolsky B, Rosen N (1935). Can quantum-mechanical description of physical reality be considered complete? Phys. Rev. 4:777-780 .

Gardner CL (1994). The quantum hydrodynamic model for semiconductor devices. SIAM. J. Appl. Math. 54:409.

Greenberger DM, Horne MA, Shimony A, Zeilinger A (1990). Bell's theorem without inequalities. Am. J. Phys. 58(12):1131-43.

Guerra F, Ruggero P (1973). New interpretation of the euclidean-Marcov field in the framework of physical Minkowski space-time. Phys rev. Lett. 31:1022 .

Jánossy L (1962). Zum hydrodynamischen Modell der Quantenmechanik. Z. Phys. 169(79):8.

Jona G, Martinelli F, Scoppola E (1981). New approach to the semiclassical limit of quantum mechanics. Comm. Math. Phys. 80:233.

Lombardo FC, Villar PI (2005). Decoherence induced by zero-point fluctuations in quantum Brownian motion. Phys. Lett. A. 336:16–24.
Madelung E (1926). Quanten theorie in hydrodynamische form (Quantum theory in the hydrodynamic form). Z. Phys. 40: 322-326.
Mariano A, Facchi P, Pascazio S (2001). Decoherence and Fluctuations in Quantum Interference Experiments, Fortschr. Phys. 49(10-11):1033–1039.
Maudlin T (1994). Quantum Non-Locality and Relativity: Metaphysical Intimations of Modern Physics, Cambridge, Massachusetts: Blackwell.
Morato LM, Ugolini S (2011). Stochastic description of a Bose–Einstein Condensate. Annales Henri Poincaré. 12(8):1601-1612.
Nelson E (1985). Quantum Fluctuations (Princeton University Press, New York.
Nelson E (1967). Dynamical Theory of Brownian Motion (Princeton University Press, London.
Oppenheim J, Wehner S (2007). The uncertainty principle determines the non-locality of quantum mechanics. Phys. Rev. Lett.103:1072-1074.
Ozawa M (2003). Universally valid reformulation of the Heisenberg uncertainty principle on noise and disturbance in measurement, Phys. Rev. A; 67:042105 (6).
Parisi G, Wu YS (1981). Perturbation Theory Without Gauge Fixing. Sci. Sin. P. 24.
Popescu S, Rohrlich D (1994). Nonlocality as an axiom". Foundation of Phys. 24(3):379–385.
Ruggiero P, Zannetti M (1981). Critical Phenomena at T=0 and Stochastic Quantization. Phys. Rev. Lett. 47: 1231.
Ruggiero P, Zannetti M (1983a). Microscopic derivation of the stochastic process for the quantum Brownian oscillator. Phys. Rev. A (28):987**.**
Ruggiero P, Zannetti M (1983b). Quantum-classical crossover in critical dynamics. Phys. Rev. B(27):3001.
Schrödinger E (1935). Die gegenwärtige Situation in der Quantenmechanik. Die Naturwissenschaften. 23:807–812, 823–828, 844–849. Hawking S, www.hawking.org.uk/does-god-play-dice.html.
Susskind L, Thorlacius L, Uglum J (1993). The stretched horizon and black hole complementarity. Phys. Rev. D. 48:3743.
t'Hooft *G (1988).* Equivalence relations between deterministic and quantum mechanical systems. J. Statistical Phys. *53: 323.*
t'Hooft G (1996). Quantization of point particles in (2+l)-dimensional gravity and spacetime discreteness, Class. Quant. Grav. 13:1023.
t'Hooft G (1999). Quantum gravity as a dissipative deterministic system. Class. Quant. Grav. 16:3263.
Terlecki G, Grun N, Scheid W (1982). Solution of the time-dependent Schrödinger equation with a trajectory method and application to H+-H scattering. Phys. Lett. 88(A):33.
von Neumann J (1932/1955). In *Mathematische Grundlagen der Quantenmechanik*, Springer, Berlin, translated into English by Beyer, R.T., Princeton University Press, Princeton, cited by Baggott, J. (2004). Beyond Measure: Modern physics, philosophy, and the meaning of quantum theory, Oxford University Press, Oxford, ISBN 0-19-852927-9, pp.144-145.
Wang C, Bonifacio P, Bingham R, Mendonca JT (2008). Detection of quantum decoherence due to spacetime fluctuations, 37th COSPAR Scientific Assembly. 13-20 July Montréal, Canada. P. 3390.
Weiner JH (1983). Statistical Mechanics of Elasticity. John Wiley & Sons, New York, pp. 315-317.
Weiner JH, Askar A (1971). Particle method for the numerical solution of the time-dependent Schrödinger Equation. J. Chem. Phys. 54:3534.
Weiner JH, Forman R (1974). Rate theory for solids. V. Quantum Brownian-motion model. Phys. Rev. B. 10:325.
Wyatt RE (2005). Quantum dynamics with trajectories: Introduction to quantum hydrodynamics, Springer, Heidelberg; P. 9.
Zwanziger D (1984). Covariant quantization of gauge fields without Gribov ambiguity. Nucl. Phys. B. 192:259.

APPENDIX A

In the QHA the eigenstates can be identified by the their stationarity that happens due the fact that the force generated by the quantum potential exactly counterbalance that one due to the Hamiltonian potential (with the initial condition $\dot{q} = 0$).

Since the quantum potential changes with the state of the system, more than one stationary state (each one with its own $V_{qu}{}^{n}$) is possible and more than one quantized eigenvalues of the energy may exist with the corresponding action values:

$$S_0{}^{n} = \int_{t_0}^{t} dt\left(\frac{p \bullet p}{2m} - V_{(q)} - V_{qu\,0}{}^{n}\right) \tag{A.0}$$

The above statements can be straightforwardly checked in the case of a linear system. For a harmonic oscillator described by the Hamiltonian $H = \frac{p^2}{2m} + \frac{m\omega^2}{2}q^2$, whose generic *n*-th eigenstate reads:

$$\psi_{n(q)} = \mathrm{n}^{\frac{1}{2}}{}_{(q,\,t)}\, exp\left[\frac{i}{\hbar}S_{(q,t)}\right] = \mathrm{H}_{n}\left(\frac{m\omega}{2\hbar}q\right) exp\left(-\frac{m\omega}{2\hbar}q^2\right), \tag{A.1}$$

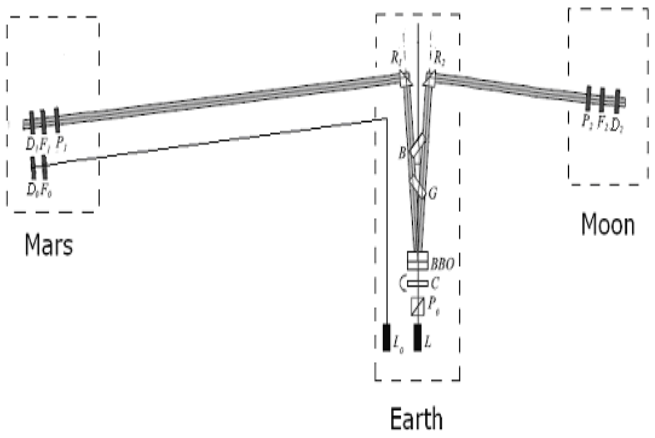

Figure 1. Schematic drawing of the experimental apparatus.

(where $\mathrm{H}_{n(\mathrm{x})}$ represents the *n*-th Hermite polynomial) the density $\mathrm{n}_{(q,\,t)}$ and the action $S_{(q,t)}$ respectively read:

$$\mathrm{n}^{1/2}{}_{(q,\,t)} = \mathrm{H}_{n}\left(\frac{m\omega}{2\hbar}q\right) exp\left(-\frac{m\omega}{2\hbar}q^2\right) \tag{A.2}$$

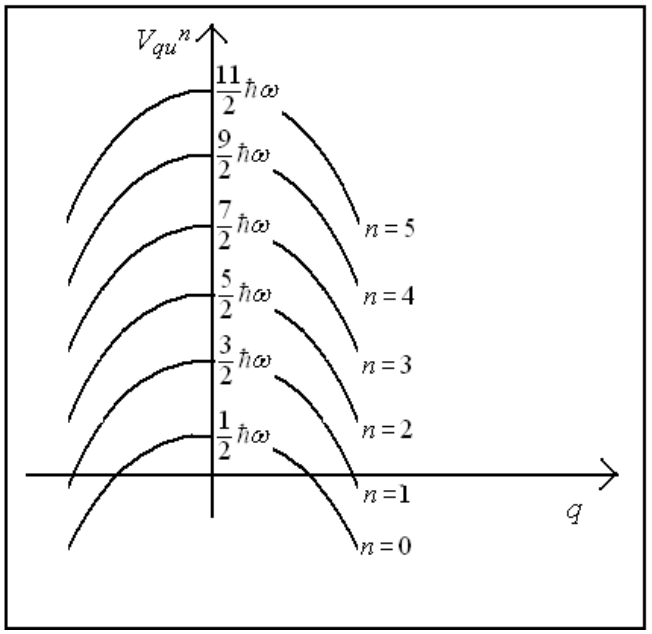

Figure 2. The repulsive quantum potential for the firsts five eigenstates of a harmonic oscillator.

$$S_{(q,t)} = S_{(t)}\,, \tag{A.3}$$

leading to the quantum potential of the *n*-th eigenstate (Figure 2)

$$\begin{aligned} V_{qu}{}^{n} &= -\left(\frac{\hbar^2}{2m}\right)\mathrm{n}^{1/2}\nabla \bullet \nabla \mathrm{n}^{1/2} \\ &= -\frac{m\omega^2}{2}q^2 + \left[n\left(\frac{\frac{m\omega}{\hbar}\mathrm{H}_{n-1} - 2(n-1)\mathrm{H}_{n-2}}{\mathrm{H}_n}\right) + \frac{1}{2}\right]\hbar\omega \\ &= -\frac{m\omega^2}{2}q^2 + \left(n + \frac{1}{2}\right)\hbar\omega \end{aligned} \tag{A.4}$$

where it has been used the recurrence formula of the Hermite polynomials

$$\mathrm{H}_{n+1} = \frac{m\omega}{\hbar}q\mathrm{H}_n - 2n\mathrm{H}_{n-1}\,, \tag{A.5}$$

that gives the following energy eigenvalues

$$\begin{aligned} E_n = \langle\psi_n | H | \psi_n\rangle &= \int_{-\infty}^{\infty} \mathrm{n}_{(q,\,t)}\left[\frac{m\omega^2}{2}(q-\underline{q})^2 + V_{qu}{}^{n} + \frac{m}{2}|\dot{q}|^2\right] \\ &= \int_{-\infty}^{\infty} \mathrm{n}_{(q,\,t)}\left[\frac{m\omega^2}{2}(q-\underline{q})^2 + V_{qu}{}^{n} + \frac{1}{2m}|\nabla S_{(q)}|^2\right] \\ &= \int_{-\infty}^{\infty} \mathrm{n}_{(q,\,t)}\left[\frac{m\omega^2}{2}(q-\underline{q})^2 - \frac{m\omega^2}{2}(q-\underline{q})^2 + \left(n + \frac{1}{2}\right)\hbar\omega\right] = \left(n + \frac{1}{2}\right)\hbar\omega \end{aligned} \tag{A.6}$$

as well as:

$$\dot{p} = -\nabla (H + V_{qu}) = -\nabla ((n + \frac{1}{2})\hbar\omega) = 0 , \quad (A.7)$$

$$\dot{q} = \frac{\nabla S_{(q,t)}}{m} = 0 , \quad (A.8)$$

$$S_0{}^n = \int_{t_0}^{t} dt(\frac{p \bullet p}{2m} - V_{(q)} - V_{qu_0}{}^n) = E_n(t - t_0) \quad (A.9)$$

APPENDIX B

Large-distance quantum force

To obtain the macro-scale form of equations (47) we need to evaluate the large-scale limit of the quantum force $\dot{x}_{qu} \equiv -\nabla_q V_{qu}$ in it. The behavior of $\mathrm{n}^{1/2}$ determines the quantum potential (QP) in (5). For sake of simplicity, we discuss the one-dimensional case of localized state with $\mathrm{n}^{1/2}$ that at large distance goes like:

$$\lim_{|q|\to\infty} \mathrm{n}^{1/2} \propto exp[-P^k(q)] \quad (B.1)$$

where $P^k{}_{(q)}$ is a polynomial of degree equal to *k*, $z_q = \gamma^{-1} q$ is the macroscopic variable (where $\gamma = \frac{\Delta q}{\lambda_q}$, where Δq is the macro-scale resolution) and λ_q is the range of the QP interaction. By using (B.1), the QP (5) at large scale reads:

$$\lim_{\gamma\to\infty} V_{qu} = \lim_{\gamma\to\infty} -k^2\gamma^{-\phi} z_q{}^{1-\phi} + k(k-1)\gamma^{-(1.5+\phi)} z_q{}^{-(3+\phi)/2} \quad (A.2)$$

where $\phi = 3 - 2k$.

Thence, for $k < \frac{3}{2}$ (that is, $\phi > 0$) $\forall\ z_q \neq 0$ finite, the quantum force $-\nabla_q V_{qu}$ at large scale (that is, $\gamma \to \infty,\ q = \gamma z_q \to \infty$) reads:

$$\lim_{\gamma\to\infty (z_q finite)} -\nabla V_{qu} = \lim_{q\to\infty} 2k^2(k-1)(\gamma z_q)^{-\phi} + k(k-1)(k-2)(\gamma z_q)^{-1/2(3+2\phi)} z_q{}^{1/2\phi} \approx 2k^2(k-1)(\gamma z_q)^{-\phi} = 0 \quad (B.3)$$

Moreover, since the integral:

$$\int_0^\infty | q^{-1}\nabla V_{qu} | dq \cong Const + \alpha \int_{q_0}^\infty | \frac{1}{q^{1+\phi}} | dq < \infty \quad (B.4)$$

converges for $\phi > 0$, (B.4) tells us if the QP force is negligible on large scale as given by (B.3). Therefore, finite values of the mean weighted distance:

$$\lambda_q = 2 \frac{\int_0^\infty | q^{-1} \frac{\partial V_{qu}}{\partial q} | dq}{\lambda_c{}^{-1} | \frac{\partial V_{qu}}{\partial q} |_{(q=\lambda_c)}} , \quad (B.5)$$

warrants the vanishing of QP at large distance and, hence, it can be assumed as an evaluation of the quantum potential range of interaction.

It is worth mentioning that condition (B.4) is not satisfied by linear systems whose eigenstates have $\phi = -1$ (22), so that $\lambda_q = \infty$ and they cannot admit the classical limit.

It is also worth noting that condition (B.4), obtained for $\mathrm{n}^{1/2}$ owing the form (B.1), also holds in the case of oscillating wave functions whose modulus is of type:

$$\lim_{|q|\to\infty} \mathrm{n}^{1/2} = | q^m \sum_n a_n \, exp[iA_n{}^p{}_{(q)}] \} exp[-P^k{}_{(q)}] | \quad (B.6)$$

where $A_n{}^p{}_{(q)}$ are polynomials of degree equal to *p*. In this case, in addition to the requisite $0 \le k < \frac{3}{2}$, the conditions $m \in \Re$ and $p \le 1$ are required to warrant (B.4) (38).

For instance, the Lennard-Jones-type potentials holds $\lim_{|q|\to\infty} A_n{}^p{}_{(q)}{}_{(q)} \propto q$ and, hence, they own λ_q finite.

In the multidimensional case, λ_q depends by the path of integration Σ and (B.5) reads:

$$\lambda_q = 2 \frac{\int_{\Sigma r=0}^{\Sigma r=\infty} r_{(\Sigma)}{}^{-1} | \frac{\partial V_{qu}}{\partial q_i} | \bullet d\Sigma_i}{\lambda_c{}^{-1} | \frac{\partial V_{qu}}{\partial r} |_{(r_{(\Sigma)}=\lambda_c)}} \quad (B.7)$$

where $r = |q|$ and $d\Sigma_i$ is the incremental vector tangent to Σ.

Since, the physical meaning of λ_q must be independent by the path of integration (we know that $\frac{\partial V_{qu}}{\partial q_i}$ is integrable but do we do not know nothing about the integrability of $r_{(\Sigma)}^{-1} | \frac{\partial V_{qu}}{\partial q_i} |$) in order to well define λ_q the fixation of the integral path is needed. If we choose the integration path $\Sigma = r m_i$ where m_i is a generic versor, λ_q reads:

$$\lambda_{q(m_i)} = 2 \frac{\int_{r=0}^{\infty} r^{-1} | \frac{\partial V_{qu}}{\partial r} |_{(q = r m_i)} dr}{\lambda_c^{-1} | \frac{\partial V_{qu}}{\partial r} |_{(q = \lambda_c m_i)}} \qquad \text{(B.8)}$$

Moreover, since in order to evaluate at what distance the quantum force becomes negligible whatever is the direction of the versor m_i, among the values of (B.8) we must consider the maximum one so, finally, λ_q reads:

$$\lambda_q = Max\left\{ 2 \frac{\int_{r=0}^{\infty} r^{-1} | \frac{\partial V_{qu}}{\partial r} |_{(q = r m_i)} dr}{\lambda_c^{-1} | \frac{\partial V_{qu}}{\partial r} |_{(q = \lambda_c m_i)}} \right\} \qquad \text{(B.9)}$$

B.1: QUANTUM potential characteristics

In order to elucidate the interplay between the Hamiltonian potential and the quantum potential, that together define the quantum evolution of the particle, we observe that the quantum potential is primarily defined by the PD.

Fixed the PD at the initial time, then the Hamiltonian potential and the quantum one determine the evolution of the PD in the following instants that on its turn modifies the quantum potential.

A Gaussian PD has a parabolic repulsive quantum potential, if the Hamiltonian potential is parabolic too (the free case is included), when the PD wideness adjusts itself to produce a quantum potential that exactly compensates the force of the Hamiltonian one, the Gaussian states becomes stationary (eigenstates). In the free case, the stationary state is the flat Gaussian (with an infinite variance) so that any free Gaussian PD expands itself following the ballistic dynamics of quantum mechanics since the Hamiltonian potential is null and the quantum one is a quadratic repulsive one.

From the general point of view, we can say that if the Hamiltonian potential grows faster than a harmonic one, the wave equation of a self-state is more localized than a Gaussian one and this leads to a stronger-than a quadratic quantum potential.

On the contrary, a Hamiltonian potential that grows slower than a harmonic one will produce a less localized PD that decreases slower than the Gaussian one, so that the quantum potential is weaker than the quadratic one and it may lead to a finite quantum non-locality length (B.5).

More precisely, as shown above, the large distances exponential-decay of the PD given by (B.1) with *k*<3/2 is a sufficient condition to have a finite quantum non-locality length (20).

In absence of noise, we can identify three typologies of quantum potential interactions (in the uni-dimensional case): *k*> 2 strong quantum potential that leads to quantum force that grows faster than linearly and λ_q is infinite (*super-ballistic* expansion for the free particle PD) and reads:

$$\lim_{|q| \to \infty} \frac{\partial V_{qu}}{\partial q} \propto q^{1+\varepsilon} . \ (\varepsilon > 0) \qquad \text{(B.10)}$$

k = 2 that leads to quantum force that grows linearly

$$\lim_{|q| \to \infty} \frac{\partial V_{qu}}{\partial q} \propto q \qquad \text{(B.11)}$$

and λ_q is infinite (*ballistic* expansion for the free particle PD); 2 > *k* ≥ 3/2 "middle quantum potential"; the integrand of (B.4) will result:

$$Cons\ tan\ t > \lim_{|q| \to \infty} | q^{-1} \frac{\partial V_{qu}}{\partial q} | > q^{-1} . \qquad \text{(B.12)}$$

The quantum force remains finite or even becomes vanishing at large distance but λ_q may be still infinite (*under-ballistic* expansion for the free particle PD).

k < 3/2 "week quantum potential" interaction leading to quantum force that becomes vanishing at large distance following the asymptotic behavior:

$$\lim_{|q| \to \infty} | q^{-1} \frac{\partial V_{qu}}{\partial q} | > q^{-(1+\varepsilon)}, \varepsilon > 0 \qquad \text{(B.13)}$$

with a finite λ_q for T ≠ 0 (*asymptotically vanishing* expansion for the free particle PD).

B.2 Pseudo-Gaussian particle

Gaussian particles generate a quadratic quantum potential that is not vanishing at large distance and hence cannot lead to macroscopic local dynamics. Nevertheless, imperceptible deviation by the perfect Gaussian PD may possibly lead to finite quantum non-locality length. Particles that are inappreciably less localized than the Gaussian ones (let's name them as pseudo-Gaussian) own $\frac{\partial V_{qu}}{\partial q}$ that can sensibly deviate by the linearity so that the quantum non-locality length may be finite.

We have seen above that for k < 3/2 (when the PD decreases slower than a Gaussian) a finite range of interaction of the quantum potential λ_q is possible.

The Gaussian shape is a physically good description of particle localization, but irrelevant deviations from it, at large distance, are decisive to determine the quantum non-locality length.

For instance, let's consider the pseudo-Gaussian wave-function type:

$$n = n_0 \exp\left[-\frac{(q-\underline{q})^2}{\underline{\Delta q^2}\left[1+\left[\frac{(q-\underline{q})^2}{\Lambda^2 f(q-\underline{q})}\right]\right]}\right] \quad \text{(B.14)}$$

where $f(q-\underline{q})$ is an opportune regular function obeying to the condition:

$$\Lambda^2 f(0) >> \underline{\Delta q^2} \text{ and } \lim_{|q-\underline{q}|\to\infty} f(q-\underline{q}) << \frac{(q-\underline{q})^2}{\Lambda^2}. \quad \text{(B.15)}$$

For small distance it holds

$$(q-\underline{q})^2 << \Lambda^2 f(q-\underline{q}) \quad \text{(B.16)}$$

and the localization given by the PD is physically indistinguishable from a Gaussian one, while for large distance we obtain the behavior:

$$\lim_{|q-\underline{q}|\to\infty} n = n_0 \exp\left[-\frac{\Lambda^2 f(q-\underline{q})}{\underline{\Delta q^2}}\right]. \quad \text{(B.17)}$$

For instance, we may consider the following examples

a)

$$f(q-\underline{q}) = 1 \quad \text{(B.18)}$$

$$\lim_{|q-\underline{q}|\to\infty} n = n_0 \exp\left[-\frac{\Lambda^2}{\underline{\Delta q^2}}\right]; \quad \text{(B.19)}$$

(b)

$$f(q-\underline{q}) = 1 + |q - \underline{q}| \quad \text{(B.20)}$$

$$\lim_{|q-\underline{q}|\to\infty} n = n_0 \exp\left[-\frac{\Lambda^2 |q-\underline{q}|}{\underline{\Delta q^2}}\right]; \quad \text{(B.21)}$$

(c)

$$f(q-\underline{q}) = 1 + ln[1+|q-\underline{q}|^g] \approx ln[|q-\underline{q}|^g] \ (0<g<2) \quad \text{(B.22)}$$

$$\lim_{|q-\underline{q}|\to\infty} n \approx n_0 |q-\underline{q}|^{-g\frac{\Lambda^2}{\underline{\Delta q^2}}}; \quad \text{(B.23)}$$

(d)

$$f(q-\underline{q}) = 1 + |q-\underline{q}|^g \quad (0< g <2) \quad \text{(B.24)}$$

$$\lim_{|q-\underline{q}|\to\infty} n = n_0 \exp\left[-\frac{\Lambda^2 |q-\underline{q}|^g}{\underline{\Delta q^2}}\right] \quad \text{(B.25)}$$

All cases (a-d) lead to a finite quantum non-locality length λ_q.

In the case (d) the quantum potential for $|q-\underline{q}| \to \infty$ reads:

$$\lim_{|q-\underline{q}|\to\infty} V_{qu} = \lim_{|q-\underline{q}|\to\infty} -\left(\frac{\hbar^2}{2m}\right)|\psi|^{-1}\nabla_q\cdot\nabla_q|\psi| \quad (0<g<2) \quad \text{(B.26)}$$
$$= -\left(\frac{\hbar^2}{2m}\right)\left[\frac{\Lambda^4 g^2 (q-\underline{q})^{2(h-1)}}{(2\underline{\Delta q^2})^2} - \frac{\Lambda^2 g(g-1)(q-\underline{q})^{g-2}}{2\underline{\Delta q^2}}\right]$$

leading, for 0< g <2, to the quantum force:

$$\lim_{|q-\underline{q}|\to\infty} -\nabla_q V_{qu} = \left(\frac{\hbar^2}{2m}\right)\left[\frac{\Lambda^4 g^2 (2g-1)(q-\underline{q})^{2g-3}}{(2\underline{\Delta q^2})^2} - \frac{\Lambda^2 g(g-1)(g-2)(q-\underline{q})^{g-3}}{2\underline{\Delta q^2}}\right] \quad \text{(B.27)}$$

that for g < 3/2 gives $\lim_{|q-\underline{q}|\to\infty} -\nabla_q V_{qu} = 0$. It is interesting to note that for g =2 (linear case):

$$|\psi| = n^{1/2} = n_0{}^{1/2}\, exp[-\frac{(q-\underline{q})^2}{2\underline{\Delta q^2}}] \qquad \text{(B.28)}$$

the quantum potential is quadratic

$$lim_{|q-\underline{q}|\to\infty} V_{qu} = -(\frac{\hbar^2}{2m})[\frac{(q-\underline{q})^2}{(\underline{\Delta q^2})^2} - \frac{1}{\underline{\Delta q^2}}], \qquad \text{(B.29)}$$

and the quantum force is linear (repulsive) and reads

$$lim_{|q-\underline{q}|\to\infty} -\nabla_q V_{qu} = (\frac{\hbar^2}{2m})[\frac{2(q-\underline{q})}{(\underline{\Delta q^2})^2}] \qquad \text{(B.30)}$$

The linear form of the force exerted by the quantum potential leads to the ballistic expansion (variance that grows linearly with time) of the free Gaussian quantum states.

International Journal of Physical Sciences

Related Journals Published by Academic Journals

- *African Journal of Pure and Applied Chemistry*
- *Journal of Internet and Information Systems*
- *Journal of Geology and Mining Research*
- *Journal of Oceanography and Marine Science*
- *Journal of Environmental Chemistry and Ecotoxicology*
- *Journal of Petroleum Technology and Alternative Fuels*

academicJournals